The Astrophysical Journal, 674:742–767, 2008 February 20

THE ORIGIN OF DWARF ELLIPTICALS IN THE VIRGO CLUSTER

A. Boselli,[1] S. Boissier,[1] L. Cortese,[2] and G. Gavazzi[3]

Received 2007 May 16; accepted 2007 October 23

ABSTRACT

We study the evolution of dwarf ($L_H < 10^{9.6}\ L_{H\odot}$) star-forming and quiescent galaxies in the Virgo Cluster by comparing their UV to radio centimetric properties to the predictions of multizone chemospectrophotometric models of galaxy evolution especially tuned to take into account the perturbations induced by the interaction with the cluster intergalactic medium. Our models simulate one or multiple ram pressure stripping events and galaxy starvation. Models predict that all star-forming dwarf galaxies entering the cluster for the first time loose most, if not all, of their atomic gas content, quenching on short timescales ($\leq$150 Myr) their activity of star formation. These dwarf galaxies soon become red and quiescent, gas metal-rich objects with spectrophotometric and structural properties similar to those of dwarf ellipticals. Young, low-luminosity, high surface brightness star-forming galaxies such as late-type spirals and BCDs are probably the progenitors of relatively massive dwarf ellipticals, while it is likely that low surface brightness Magellanic irregulars evolve into very low surface brightness quiescent objects hardly detectable in ground-based imaging surveys. The small number of dwarf galaxies with physical properties intermediate between those of star-forming and quiescent systems is consistent with a rapid ($<$1 Gyr) transitional phase between the two dwarf galaxy populations. These results, combined with statistical considerations, are consistent with the idea that most of the dwarf ellipticals dominating the faint end of the Virgo luminosity function were initially star-forming systems, accreted by the cluster and stripped of their gas by one or subsequent ram pressure stripping events.

Subject headings: galaxies: clusters: individual (Virgo) — galaxies: interactions — ultraviolet: galaxies

Online material: color figures

1. INTRODUCTION

Dwarf galaxies ($M_B > -18$) are the most common objects in the nearby universe (Ferguson & Binggeli 1994). Their importance resides in the fact that they represent in cold dark matter models the building blocks of hierarchical galaxy formation (e.g., White & Rees 1978; White & Frenk 1991). Their study is thus fundamental for constraining models of galaxy formation and evolution.

Observations of dwarf galaxies, necessarily limited to the nearby universe, revealed, however, a more complex origin than that predicted by models, making this class of galaxies even more interesting. Among dwarf galaxies, dwarf ellipticals (dEs) and the less luminous dwarf spheroidals (dSph)[4] are more common than star-forming Im dwarfs and blue compact dwarfs (BCDs; Ferguson & Binggeli 1994). Originally thought of as the low-luminosity extension of bright ellipticals, several observational evidences indicate that they form an independent class of objects (Bender et al. 1992). Dwarf and giant ellipticals have Sérsic light profiles of index $1/n$, with n progressively increasing with luminosity (Graham & Guzman 2003; Gavazzi et al. 2005b). The color-magnitude relations measured using resolved stars in Local Group dwarf spheroidals (Mateo 1998; Grebel 1999), the optical (Conselice et al. 2003a) and UV (Boselli et al. 2005b) integrated color-magnitude relations, the subsolar [α/Fe] ratios (van Zee et al. 2004a), and the UV to near-IR spectral energy distribution (SED) of dEs in the Virgo Cluster (Gavazzi et al. 2002a), however, all indicate a more gradual star formation history with recent episodes of activity in these low-luminosity quiescent systems than in massive ellipticals. This constitutes the first evidence against their very old origin. A further disagreement with model predictions is that, although more frequent than bright galaxies, their number density is still significantly smaller than predicted by hierarchical models of galaxy formation for the field luminosity function (Kauffmann et al. 1993; Cole et al. 1994; Somerville & Primack 1999; Nagashima et al. 2005) or for the Local Group (Klypin et al. 1999; Bullock et al. 2000).

The strong similarities in the structural properties of star-forming and quiescent dwarf galaxies in the nearby universe, namely, their similar optical morphology and light profiles (both roughly exponentials), suggested that dwarf ellipticals might result from gas removal and subsequent suppression of star formation in gas-rich dwarf galaxies. Gas removal might result either from its blowout due to the kinetic energy injected into the interstellar medium (ISM) by supernova explosion following a strong burst of star formation (Dekel & Silk 1986; Vader 1986; Yoshii & Arimoto 1987), from gas exhaustion through subsequent episodes of star formation (Davies & Phillipps 1988), or from external perturbations induced by the hostile environment in which galaxies evolve. External perturbations include tidally induced mass loss in high-speed encounters (Moore et al. 1998), tidal stirring (Mayer et al. 2001a, 2001b), and ram pressure stripping induced by nearby companions (Lin & Faber 1983) or by the hot intergalactic medium (IGM) in massive clusters (van Zee et al. 2004b).

Several observational evidences favor the environmental scenario against the gas blowout due to supernova explosions. The clearest indication that the environment plays an important role in the formation and evolution of dwarfs is the morphology segregation effect (Dressler 1980), which extends to low-luminosity systems (Binggeli et al. 1988, 1990; Ferguson & Binggeli 1994). Furthermore, it has been recently claimed that the removal of the ISM through supernova winds is quite difficult in low-luminosity, dark matter–dominated systems (Mac Low & Ferrara 1999; Ferrara & Tolstoy 2000; Silich & Tenorio-Tagle 1998, 2001). The discrete

[1] Laboratoire d'Astrophysique de Marseille, F-13376 Marseille, France.
[2] School of Physics and Astronomy, Cardiff University, 5, The Parade, Cardiff CF24 3YB, UK.
[3] Universita degli Studi di Milano-Bicocca, 20126 Milan, Italy.
[4] Unless specified, in the following we indicate with dE all quiescent dwarf galaxies, including dSph.

star formation history of several dwarf galaxies in the Local Group, as deduced by the analysis of their color-magnitude relation (Mateo 1998; Grebel 1999), is a further indication that dwarf spheroidals can retain their ISM through several episodes of star formation.

Another observational evidence favoring the transformation of star-forming galaxies into quiescent dwarf ellipticals is the presence of rotationally supported (Pedraz et al. 2002; Geha et al. 2003; van Zee et al. 2004b) and/or H I gas-rich (Conselice et al. 2003b; van Zee et al. 2004b) dEs in the Virgo Cluster. Recent studies based on SDSS imaging and spectroscopic data have shown that ~50% of the bright end of the dE galaxy population in the Virgo Cluster is characterized by disk features such as spiral arms or bars, this fraction decreasing down to ~5% at lower luminosities (Lisker et al. 2006b; see also Graham et al. 2003). Meanwhile, ~15% of the bright dEs in Virgo have blue centers revealing a recent activity of star formation. From a statistical point of view, the line-of-sight velocity distribution of dEs inside clusters is similar to that of late-type galaxies suggesting a recent infall (Binggeli et al. 1993; Conselice et al. 2001).

Not all observational evidences, however, are consistent with the transformation of dwarf star-forming galaxies into dwarf ellipticals under the effect of the environment. To reproduce the color-magnitude relation of dwarf ellipticals, it has been claimed that Magellanic irregulars should have faded ~1.5 mag in the B band, thus reaching surface brightnesses weaker than $\mu(B)_e = 25$ mag arcsec^{-2}, values significantly smaller than the observed ones (Bothun et al. 1986). Most of the bright dwarf ellipticals in the Virgo Cluster have a bright nucleus (Binggeli et al. 1985; Ferguson & Binggeli 1994) of small size, as shown by *Hubble Space Telescope* (*HST*) observations (~4 pc; Côté et al. 2006), while dwarf irregulars do not. While both dwarf irregulars and dwarf ellipticals follow different metallicity-luminosity relations, dwarf spheroidals are more metal-rich than dwarf irregulars at the same optical luminosity (Grebel et al. 2003 and references therein). The flattening distribution of nonnucleated dEs is similar to that of late-type spirals, Im dwarfs, and BCDs (Binggeli & Popescu 1995). This class of objects, however, is significantly less round than nucleated systems. Although they exist, the fraction of objects belonging to the intermediate dIrr/dE transition class is too small. Furthermore, a simple transformation of Im galaxies recently infalling in the cluster into dEs does not seem to reproduce the observed difference in the cluster and field luminosity functions (Conselice 2002). Other strong constraints against the transformation of star-forming into quiescent dwarfs are given by the studies of globular clusters, taken as a probe of the early phases of galaxy formation. The specific frequency of globular clusters in dwarf ellipticals, in fact, is significantly higher than that of star-forming galaxies. This result has been interpreted as evidence for a different formation scenario for the two galaxy populations (Miller et al. 1998; Strader et al. 2006).

With the aim of explaining these evidences, slightly different evolutionary scenarios have been proposed: cluster dwarf ellipticals might have been formed from higher surface brightness BCD galaxies (Bothun et al. 1986), or from tidally induced mass loss in multiple high-speed encounters of massive galaxies (galaxy harassment; Mastropietro et al. 2005). Alternatively, Lisker et al. (2006a, 2006b, 2007) proposed that the cluster dwarf elliptical galaxy population is composed of different subcategories of objects, of which not all have been formed from gas-stripped star-forming dwarfs. As emphasized here, the issue is still hotly debated.

A few years ago we started collecting multifrequency data covering the whole electromagnetic spectrum for galaxies in nearby clusters in order to study the effects of the environment on galaxy evolution. Up to now our research was primarily focused on the bright end of the luminosity function. Our interest covered the present and past star formation activity (Gavazzi et al. 1991, 1998, 2002a, 2006a), the atomic (Gavazzi et al. 2005a, 2006b) and molecular gas content (Boselli 1994; Boselli et al. 1994, 1997a, 2002), and the radio continuum and IR properties of cluster galaxies (Gavazzi & Boselli 1999; Gavazzi et al. 1991). The results of our analysis, combined with those obtained by other teams, are summarized in a recent review article (Boselli & Gavazzi 2006).

The aim of the present paper is to extend the multifrequency analysis to the low-luminosity end of the luminosity function with the purpose of studying the possible transformation of star-forming objects into dwarf ellipticals. This exercise is here done using a complete sample of galaxies in the Virgo Cluster. The novelty of this work compared to previous investigations is twofold: the analyzed sample has an unprecedented multifrequency spectral coverage from the UV to near-IR imaging data. Furthermore, this unique data set is compared to the predictions of multizone chemospectrophotometric models of galaxy evolution here adapted to take into account the perturbations induced by the cluster environment. The types of perturbation simulated by the models are ram pressure stripping (Gunn & Gott 1972) and starvation (Larson et al. 1980). The combination of multifrequency data with these models on the galaxies NGC 4569 (Boselli et al. 2006) and NGC 4438 (Boselli et al. 2005a) indeed indicated how powerful this method is for studying and constraining the evolution of cluster galaxies.

Our previous investigations have emphasized that the most important parameter governing the evolution is the total mass as traced by the near-IR H-band luminosity (Gavazzi et al. 1996, 2002b; Boselli et al. 2001). Below a certain mass ($L_H < 10^{9.6}\ L_{H\odot}$) we identify the sequence of dwarf galaxies that we subdivide into quiescent and star-forming disregarding their detailed morphology.

A major uncertainty in the interpretation of the multifrequency data, and in particular of those at short wavelength, is the extinction correction, which, however, is expected to be minor in low-metallicity star-forming dwarf systems (Buat & Xu 1996) and probably negligible in dwarf ellipticals. For these reasons we decided to limit the present analysis to the cluster dwarf galaxy population, leaving the discussion relative to massive galaxies to a future communication. With the aim of driving the reader's attention to the scientific results of this work, the presentation of the data set and the general description of the models are given in Appendices A and B.

2. SAMPLE AND DATA

The analysis presented in this work is based on an optically selected sample of galaxies in the Virgo Cluster ($12^h <$ R.A. $< 13^h$, $0^\circ <$ decl. $< 18^\circ$, J2000.0) extracted from the Virgo Cluster Catalogue (VCC) of Binggeli et al. (1985), with $m_B < 18$ mag (that for a distance of 17 Mpc gives $M_B \leq -13.15$), which corresponds to its completeness limit.

Although the present analysis is focused on the dwarf star-forming (Scd–Im–BCD) and quiescent (dE–dS0) galaxy populations, which we define as $L_H < 10^{9.6}\ L_{H\odot}$ (which roughly corresponds to $M_B \gtrsim -18$ mag), we also include brighter objects selecting all galaxies with $m_B < 18$ mag. These are all bona fide Virgo Cluster members, whose distances have been assigned following the subcluster membership criteria of Gavazzi et al. (1999), which are based on combined position and redshift data (now available for 83% of the objects). The adopted distance for each subgroup is 17 Mpc for cluster A, the north and east clouds,

and the southern extension; 23 Mpc for cluster B; and 32 Mpc for the W and M clouds. The selected sample includes a total of 1010 galaxies, 445 of which are classified as dE or dS0, 215 as Scd–Sd, Im, or BCD, and 45 as dE/Im or ? in the VCC. Because of their intrinsic color, the lowest *H*-band luminosities (thus the lowest total dynamical masses) are reached only in star-forming dwarfs.

Model predictions are compared to UV to near-IR imaging and spectroscopic data collected thanks to our own observations (optical, near-IR, and Hα imaging, optical integrated spectroscopy) or from different ground-based (SDSS) and space-based (*GALEX)* missions, as well as from multifrequency data available in the literature. The detailed description of the used data set is given in Appendix A.

3. THE EVOLUTION OF LOW-LUMINOSITY LATE-TYPE GALAXIES IN CLUSTERS: MODEL PREDICTIONS

The evolution of galaxies is traced using the multizone chemical and spectrophotometric models of Boissier & Prantzos (2000), updated with an empirically determined star formation law (Boissier et al. 2003) relating the star formation rate to the total gas surface densities, and modified to simulate the effects induced by the interaction with the cluster IGM. In the starvation scenario (Larson et al. 1980; Balogh et al. 2000; Treu et al. 2003), the cluster acts on large scales by removing any extended gaseous halo surrounding the galaxy, preventing further infall of such gas onto the disk. The galaxy then becomes anemic simply because it exhausts the gas reservoir through ongoing star formation. Starvation has been simulated by stopping infall in the model.

The ISM of galaxies crossing the cluster with velocities of $\sim$1000 km s^{-1} can be removed by the ram pressure exerted by the hot and dense IGM (Gunn & Gott 1972). Gas removal induces a quenching of the star formation activity (Boselli & Gavazzi 2006). The ram pressure stripping event is simulated by assuming a gas-loss rate inversely proportional to the potential of the galaxy, with an efficiency depending on the IGM gas density radial profile of the Virgo Cluster given by Vollmer et al. (2001). The details of the models are given in Appendix B. Here we present their results.

3.1. *The Starvation Scenario*

The total gas content, the activity of star formation, and the metallicity of dwarf galaxies are barely affected by starvation unless the interaction started a long time ago, as shown for a model galaxy of rotational velocity $V_C = 55$ km s^{-1} and spin parameter $\lambda = 0.05$ (Figs. 1–4). H I deficiencies of $\sim$0.8, similar to the average value of Virgo galaxies within the virial radius of the cluster, can be obtained only if starvation started more than 6 Gyr ago (see Fig. 1).

Gas removal induces a mild decrease of the star formation activity (Fig. 1). For this reason galaxies suffering starvation for a long time are redder than similar unperturbed objects, in particular in those color indices tracing significantly different stellar populations (FUV $-$ *B*, FUV $-$ *H*, *B* $-$ *H*; Fig. 2). The FUV $-$ NUV color index is barely affected because starvation acts on longer timescales than the lifetimes of the stellar populations emitting in the two UV filters[5] ($\leq 10^8$ yr) and does not totally eliminate these

[5] The UV emission of star-forming galaxies is due to relatively young and massive A stars (Boselli et al. 2001). The UV emission of dwarf ellipticals is due to a residual star formation activity since it does not show, as in massive ellipticals, the UV upturn due to hot, evolved stars (Boselli et al. 2005b).

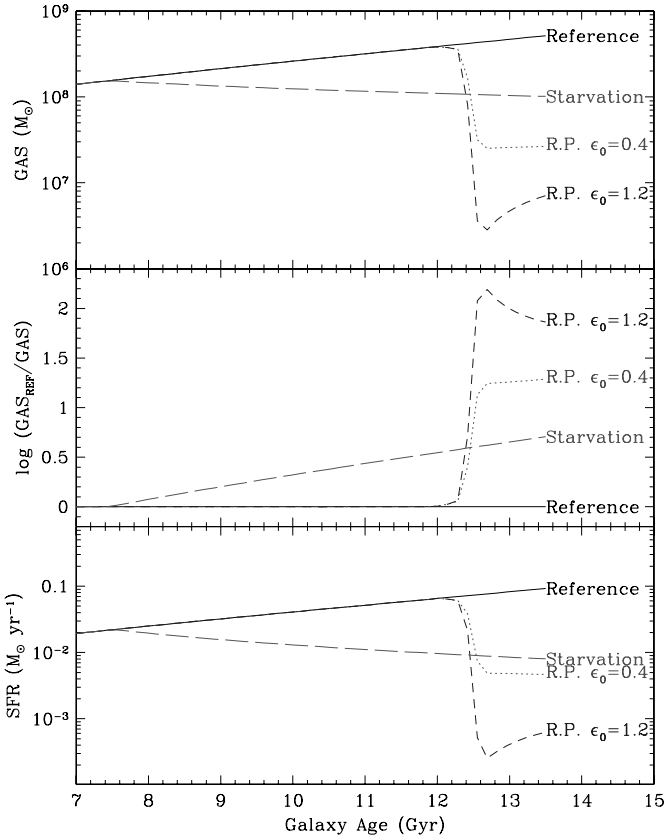

FIG. 1.—Evolution with time of the total gas content (*top*), of the unperturbed-to-perturbed gas mass ratio (*middle*; in logarithmic scale: this entity corresponds to the H I deficiency parameter), and of the star formation rate (*bottom*) for a galaxy with rotational velocity $V_C = 55$ km s^{-1} and spin parameter $\lambda = 0.05$. The solid line shows the unperturbed model (reference), the long-dashed line a starvation model for a galaxy-cluster interaction started 6 Gyr ago, the dotted line a ram pressure stripping model with an efficiency of $\epsilon_0 = 0.4\ M_\odot$ kpc^{-2} yr^{-1}, and the short-dashed line a ram pressure stripping model with an efficiency of $\epsilon_0 = 1.2\ M_\odot$ kpc^{-2} yr^{-1}. The ram pressure stripping event in both of these models started 1 Gyr ago ($t_{rp} = 1$ Gyr). The increase with time of the total gas content and of the star formation activity for an unperturbed galaxy is due to gas infall. [*See the electronic edition of the Journal for a color version of this figure*.]

populations as significant amounts of star formation, although reduced, still take place.

Gas metallicity increases more than in the unperturbed case since newly formed metals are diluted in smaller amounts of gas, and since the metallicity is not reduced by the infall of pristine gas (Fig. 3).

The effects of starvation on the structural properties of galaxies (provided that the interaction started a long time ago) are major. The decrease of the surface brightness is expected to be $\sim$1 mag in the *H* band to $\sim$3 mag in the FUV band for an interaction that started 6 Gyr ago (Fig. 4). The effect would be significantly smaller for a recent interaction.

The effects of starvation on the effective radius are minor since starvation is a global effect and thus does not depend on radius. Nevertheless, an effect on the effective radius is visible, especially at short wavelengths. The reason is the radial dependence of infall (galaxies are formed inside out in our model). When the starvation starts, infall has occurred in the inner zones, where a relatively large amount of gas can be found (and thus a high level of star formation and UV surface brightness). This gas is progressively depleted by star formation, leading to a decrease of the inner surface brightness, while the outer parts, where the star formation is low because of the low amount of gas present,

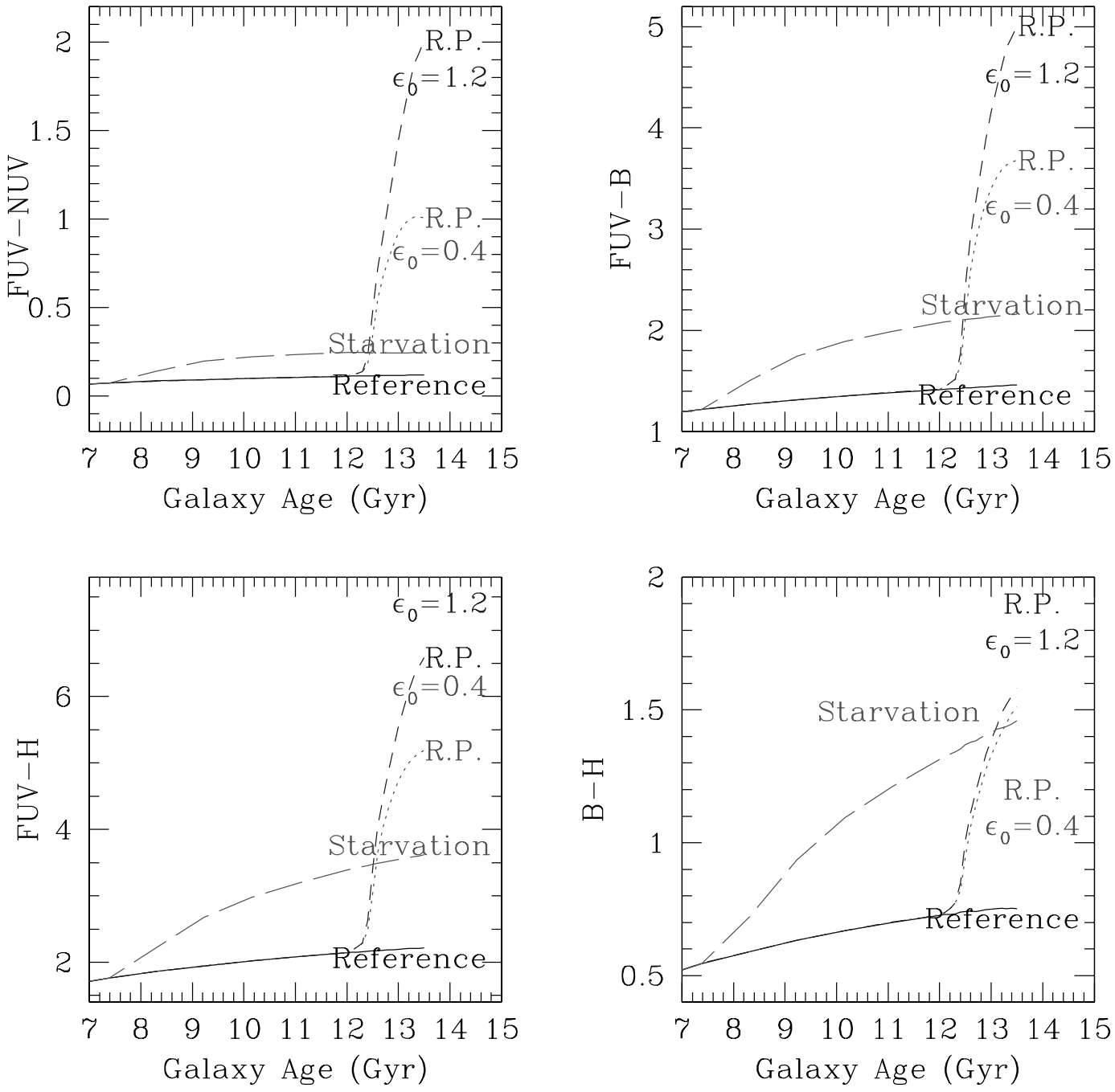

FIG. 2.—Evolution of different color indices (in the AB system) for a galaxy with rotational velocity $V_C = 55$ km s^{-1} and spin parameter $\lambda = 0.05$. Symbols are as in Fig. 1. [*See the electronic edition of the Journal for a color version of this figure*.]

dim at a lower rate. The net effect is an increase in the effective radius.

3.2. *The Ram Pressure Stripping Scenario*

The effects of a ram pressure stripping event that started 1 Gyr ago ($t_{\rm rp} = 1$ Gyr) on the evolution of total gas content, star formation activity, stellar populations (UV to near-IR color indices), metallicity, and structural (effective radius and surface brightness) parameters of dwarf galaxies as predicted by our models are also shown in Figures 1–4. Because of the shallow potential well of dwarf galaxies, most of their gas is efficiently removed on very short timescales (∼150 Myr), leading to the formation of extremely gas-deficient objects with H I deficiencies ∼2 for $\epsilon_0 = 1.2\,M_\odot$ kpc^{-2} yr^{-1}, or ∼1.2 for $\epsilon_0 = 0.4\,M_\odot$ kpc^{-2} yr^{-1} (ϵ_0 is the parameter that quantifies the efficiency of the process of ram pressure stripping; see Appendix B).

As a consequence of this lack of gas, star formation abruptly decreases by a factor of ∼10–100 and continues at a very low level afterward. In the $\epsilon_0 = 1.2\,M_\odot$ kpc^{-2} yr^{-1} model, the gas content progressively increases after the interaction as stars of small masses reach their end of life point and return more gas to the ISM (we do not use the instantaneous recycling approximation). The star formation rate is fed by this recycled gas and increases as well, staying nevertheless at low levels. In models with a lower ram pressure efficiency, the recycled gas represents a small amount with respect to the one left after the interaction. As a result, this effect is not visible: the gas and the star formation rate are about constant after the event.

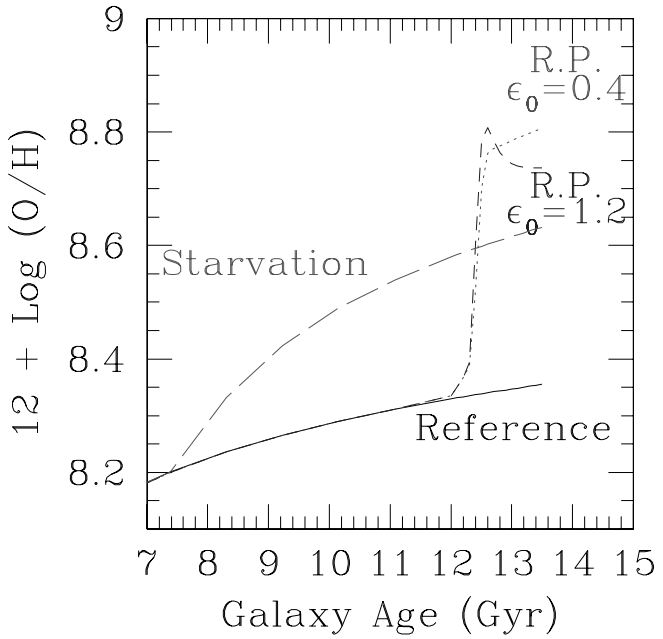

FIG. 3.—Evolution of the gas 12 + log (O/H) metallicity index for a galaxy with rotational velocity $V_C = 55$ km s^{-1} and spin parameter $\lambda = 0.05$. Symbols are as in Fig. 1. [*See the electronic edition of the Journal for a color version of this figure.*]

Stopping the star formation makes galaxies redder. Since the decrease of the star formation activity is rapid, the younger stellar populations, those emitting in the FUV and NUV filters, are the most affected: the FUV $- H$ color index, for instance, increases by $\sim$4.5 mag in 1 Gyr, while $B - H$ by only 1 mag.

As for the starvation scenario, the gas metallicity index significantly increases with time. The increase of the gas metallicity is higher during a ram pressure stripping event since virtually all the gas has been removed, while some gas is left in the disk during a starvation event. There is thus less dilution for a ram pressure event than in the occurrence of starvation.

Stopping the star formation drastically changes the structural properties of galaxies. Stripped galaxies have lower surface brightnesses and are slightly smaller with respect to unperturbed objects when observed at short wavelengths. At long wavelengths, where the emission is dominated by the evolved stellar populations, the effects are almost negligible (Fig. 4).[6]

An accurate comparison between the effects induced by ram pressure stripping and starvation on dwarf galaxy properties indicates that the former interaction is more efficient than the latter in removing gas and suppressing any star formation activity in galaxies on short timescales. To be efficient, starvation should have started several Gyr ago. Recent ram pressure stripping events, however, did not have enough time to perturb the old stellar component emitting in the near-IR.

The effects of multiple encounters on the gas content and star formation activity of a dwarf, star-forming galaxy of spin parameter $\lambda = 0.05$ and rotational velocity $V_C = 55$ km s^{-1} are shown in Figure 5. The comparison of Figure 5 with Figure 1 (single stripping event) shows how multiple interactions make galaxies even poorer of gas and, as a consequence, redder in colors than similar objects that underwent a single ram pressure stripping event. For low efficiencies, successive crossings are almost additive (some gas left on the first crossing is removed on the next one). For large efficiencies, the second crossing, occurring 1.7 Gyr after the first one, mostly removes any recycled gas, quenching a possible increase of star formation. In both cases, multiple crossing galaxies end up as redder, poorer in gas objects. A summary of the predicted perturbations induced by ram pressure stripping and starvation on the physical and structural properties of dwarf galaxies is given in Table 1.

4. MODELS VERSUS OBSERVATIONS

The multifrequency data set available for dwarf galaxies in the Virgo Cluster (see Appendix A) allows us to compare model predictions with observations.

4.1. *Gas Content*

Ram pressure stripping models are able to reproduce the H I deficient[7] galaxy population, while starvation does not (Fig. 6).[8] As previously remarked in § 3.2, ram pressure stripping can produce H I deficient massive galaxies ($L_H \sim 10^{11}\ L_{H\odot}$) such as those observed in Virgo. For a massive galaxy with $V_C = 220$ km s^{-1} and spin parameter $\lambda = 0.05$, a ram pressure stripping event that started 1 Gyr ago with $\epsilon_0 = 0.4\ M_\odot$ kpc^{-2} yr^{-1} leads to an H I deficiency of $\sim$0.8, similar to the average H I deficiency of massive spiral galaxies in the center of the Virgo Cluster (Gavazzi et al. 2005a; Boselli & Gavazzi 2006). More extreme H I deficient objects of the cluster (H I deficiency $\sim$1.4) can be produced by assuming $\epsilon_0 = 1.2\ M_\odot$ kpc^{-2} yr^{-1}. NGC 4569 can be taken as a typical object of this second category (Boselli et al. 2006).

We notice, however, that the H I emission of the ram pressure–stripped dwarf galaxy population can be hardly detected by the recent H I surveys such as ALFALFA (Giovanelli et al. 2005) and AGES (Auld et al. 2006), able to reach only galaxies with H I gas masses $\geq 10^{7.5}\ M_\odot$ (ALFALFA) or slightly smaller (AGES) at the distance of Virgo (17 Mpc) (Fig. 6, *dashed line*). Galaxies less luminous than $L_H \sim 10^{9.2}\ L_{H\odot}$ would be detected only in the case in which stripping is still underway. Since the gas stripping event is short in time ($\sim$150 Myr), we expect that these objects are extremely rare.

4.2. *Stellar Populations*

Figure 7 shows several color-magnitude relations for galaxies in the Virgo Cluster. We easily recognize the well-known red and blue sequences relative to the quiescent and star-forming galaxy populations (Scodeggio et al. 2002; Gil de Paz et al. 2007; for early-type galaxies see also Visvanathan & Sandage 1977; Bower et al. 1992; for late-type galaxies see Tully et al. 1982; Gavazzi et al. 1996) and a relatively large number of objects in between these two sequences (see § 5). We remind that the reddest quiescent dwarfs might be undetected in the UV bands because of the sensitivity of *GALEX*. Model predictions clearly show that only a ram pressure stripping event (and not starvation) is able to significantly modify the colors of galaxies. As expected, the effects are more important at short than at long wavelengths, affecting

[6] In the UV, in our example of Fig. 4, the effective radius presents large variations in its value after ram pressure started. This is due to the fact that the galaxy is left with a very low amount of gas, and the effective radius becomes sensitive to two opposite effects. In a first phase, the dominant effect is that the inner disk is depleted through star formation at a larger rate than the outer disk, leading to an increase of R_e (like in the starvation case). In a second phase, the inner disk is partially replenished with recycled gas (ejected at the end of the life of long-lived stars), leading this time to a decrease of R_e.

[7] Model H I gas masses are estimated assuming that the total gas amount of star-forming galaxies is composed of $\sim$15% of molecular gas (Boselli et al. 2002) and 30% of helium, thus $M_{\rm H\,I} \sim M_{\rm gas}/1.4$.

[8] We notice that here and in the subsequent Figs. 8–10 and 12 the model tracks do not describe a time evolution, but rather show current values for models with different look-back times of a ram pressure or starvation event.

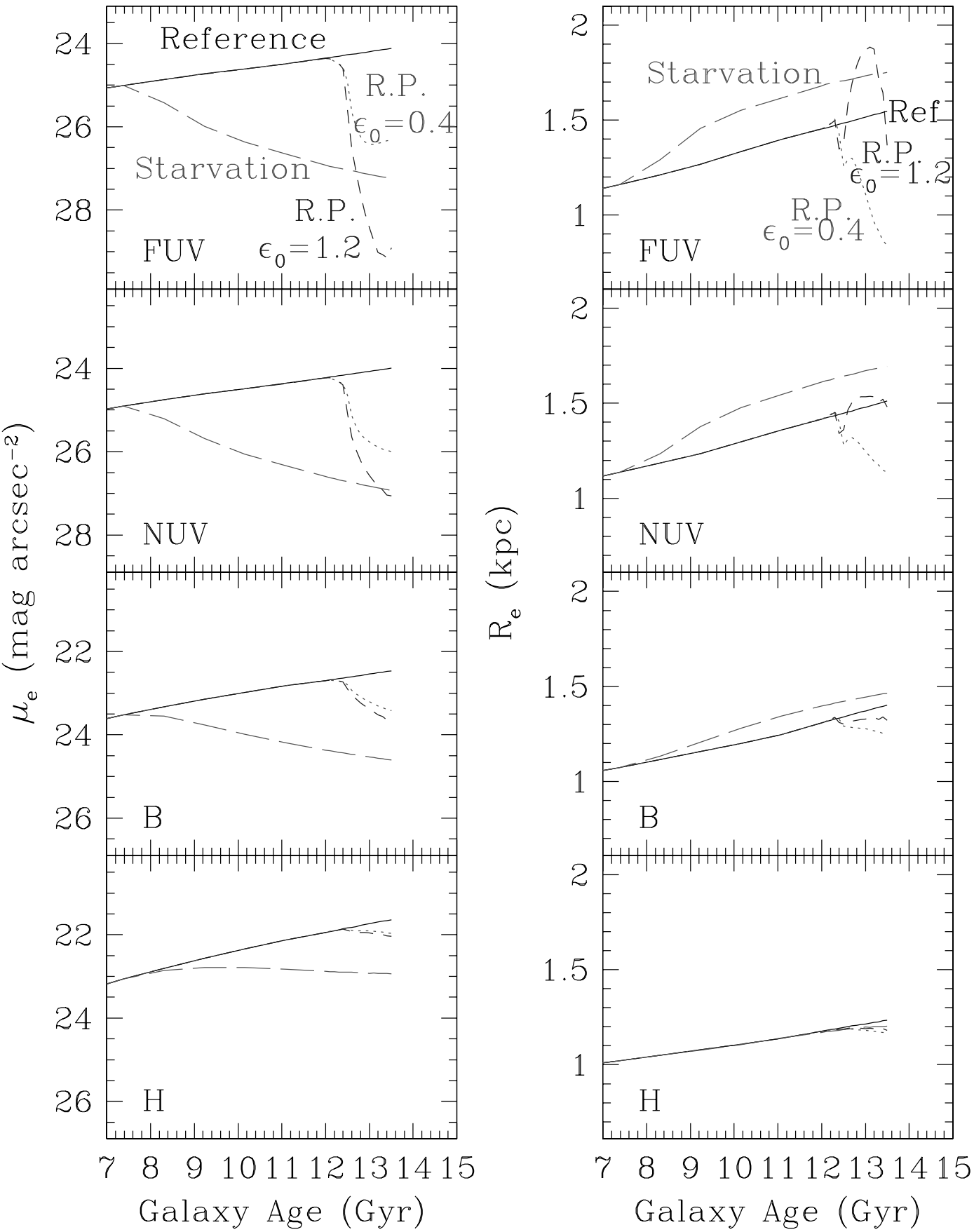

FIG. 4.— Evolution of the effective surface brightness (*left*) and radius (*right*) in different bands for a galaxy with rotational velocity $V_C = 55\,\mathrm{km\,s^{-1}}$ and spin parameter $\lambda = 0.05$. Symbols are as in Fig. 1. [*See the electronic edition of the Journal for a color version of this figure.*]

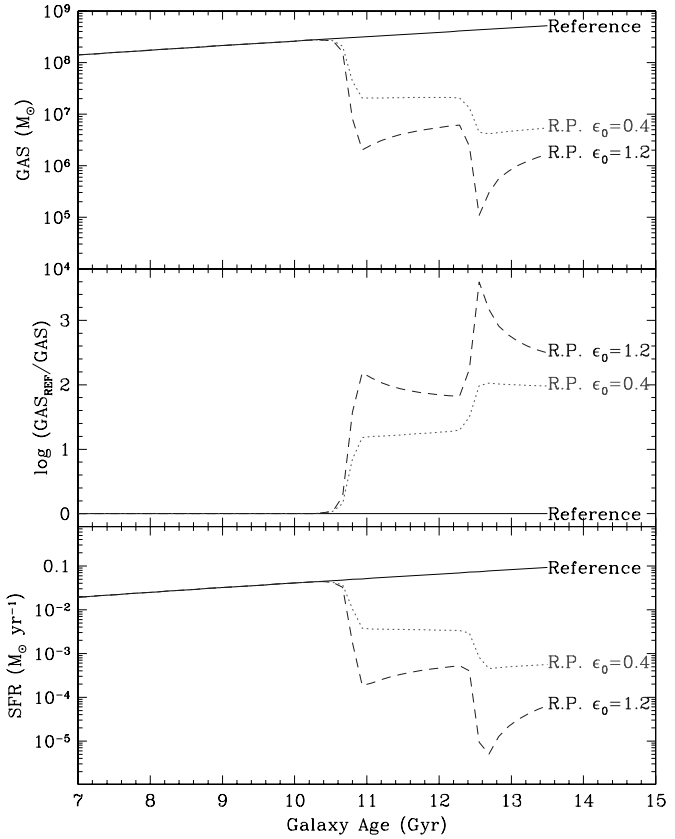

FIG. 5.—Evolution with time of the total gas content (*top*), of the unperturbed-to-perturbed gas mass ratio (*middle*), and of the star formation rate (*bottom*) for a galaxy with rotational velocity $V_C = 55$ km s^{-1} and spin parameter $\lambda = 0.05$ after two ram pressure stripping events. The solid line shows the unperturbed model (reference), the dotted line a ram pressure stripping model with an efficiency of $\epsilon_0 = 0.4\,M_\odot$ kpc^{-2} yr^{-1}, and the short-dashed line a ram pressure stripping model with an efficiency of $\epsilon_0 = 1.2\,M_\odot$ kpc^{-2} yr^{-1}. The two stripping events are delayed by 1.7 Gyr, the crossing time of late-type galaxies in the Virgo Cluster. [*See the electronic edition of the Journal for a color version of this figure.*]

more colors as, e.g., FUV − H, FUV − B than, e.g., $B - H$. The color index of bright spirals ($L_H \geq 10^{10}\,L_{H\odot}$) can increase by up to ∼1 mag in FUV − NUV and 2 mag in FUV − H or FUV − B ∼500 Myr after the interaction, making galaxies as red as the most deficient spirals located in between the red and blue sequences in the color-magnitude diagram. NGC 4569 might be one of these objects.

The effect on dwarfs is more important, making star-forming irregulars as red as dwarf ellipticals of similar luminosity in the case of an efficient gas stripping event or just after they crossed twice the cluster core (∼2 Gyr), as shown in Figure 8 (see also Fig. 13 below).

4.3. *Metallicity*

Figure 9 shows the relationship between the gas 12 + log (O/H) index and the total H-band luminosity of galaxies in the Virgo Cluster. Given the large uncertainty in both models (it is well known that metal yields are uncertain by at least a factor of 2 [see, e.g., Prantzos 2000] and chemical evolution models are somewhat degenerate due to uncertainties on, e.g., the initial mass function or star formation history) and observables (0.3 dex), it is not surprising that models for the unperturbed galaxies are slightly shifted with respect to the data. We should thus consider only relative values. It is, however, clear that all starvation and ram pressure models predict both an increase of the gas metallicity and a decrease of the total H-band luminosity consistent with the dispersion in the data. This might explain the increase of gas metallicity observed in Virgo Cluster (Vilchez 1995) and Hydra I Cluster (Duc et al. 2001) galaxies.

4.4. *Structural Properties*

The structural properties of quiescent and star-forming dwarf galaxies are compared to model predictions in Figures 10 and 11. The near-IR light concentration index C_{31} (defined as the ratio of the radii including 75% and 25% of the total light) is a quantitative indicator of the shape of the light profile in galaxies that

TABLE 1

EFFECTS OF THE INTERACTIONS WITH RESPECT TO AN UNPERTURBED MODEL

	RAM PRESSURE			STARVATION		
VARIABLE	Modification	Amount	Timescale	Modification	Amount	Timescale[a]
Gas content	∼Totally removed	Factor 10–100	≲150 Myr	Partly removed	≲10	6 Gyr
H I deficiency	Strongly deficient	1–2	≲150 Myr	Mildly deficient	≤0.5	6 Gyr
Colors	Strongly reddened	...	...	Mildly reddened	...	...
FUV − NUV	Increased	1–2 mag	≲1 Gyr	Increased	0.2 mag	6 Gyr
FUV − H	Increased	3–5 mag	≲1 Gyr	Increased	1.5 mag	6 Gyr
FUV − B	Increased	2.5–4 mag	≲1 Gyr	Increased	≲1 mag	6 Gyr
$B - H$	Increased	1 mag	≲1 Gyr	Increased	1 mag	6 Gyr
Color gradients	Blue center	1–2 mag (NUV − i)	1–5 Gyr	Red center	1 mag	Any
Star formation	Stopped	...	...	Mildly decreased	...	...
Hα EW	Drop to	∼0 Å	≲150 Myr	Drop to	∼10 Å	6 Gyr
Hβ EW	Drop to	∼2.3 Å	≲1 Gyr	Drop to	∼2.3 Å	6 Gyr
Metallicity:						
Gas	Increased	∼0.6 dex	≲200 Myr	Mildly increased	∼0.4 dex	6 Gyr
In old stars	Unchanged	...	...	Unchanged	...	...
Average stellar	Mildly reduced	0–0.15 dex	0–5 Gyr	Mildly increased	∼0.1 dex	6 Gyr
Surface brightness	Decreased	...	...	Decreased	...	...
FUV	Strongly decreased	2–5 mag	≲1 Gyr	Strongly decreased	3 mag	6 Gyr
NUV	Strongly decreased	2–3 mag	∼1 Gyr	Strongly decreased	3 mag	6 Gyr
B	Mildly decreased	1 mag	≳1 Gyr	Decreased	2 mag	6 Gyr
H	∼Constant	≲0.5 mag	≳1 Gyr	Decreased	1.5 mag	6 Gyr

[a] 6 Gyr is the look-back time for starvation in our models. For a look-back time <6 Gyr the effects induced by starvation are less important, while they are more important for a look-back time >6 Gyr.

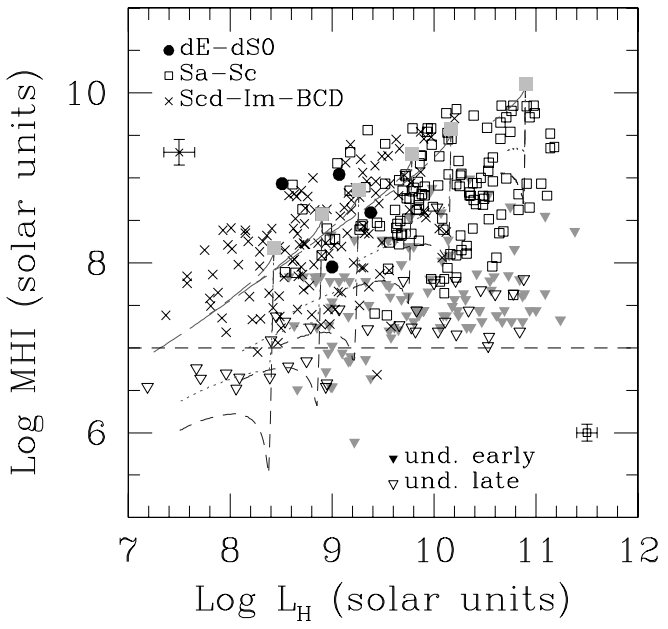

FIG. 6.—Relationship between the H I mass and the *H*-band luminosity, tracer of the total mass of galaxies, compared to model predictions for different look-back times of a ram pressure/starvation event. Open squares are for Sa–Sc galaxies, crosses for Scd–Im–BCD galaxies, and filled circles for dE–dS0 galaxies. Open triangles are upper limits for undetected late-type galaxies, gray filled triangles for undetected early-type galaxies. The dashed line indicates the region that is inaccessible to the observations with a sensitivity of 1 mJy per channel for galaxies at the distance of Virgo. Model predictions for unperturbed galaxies of spin parameter $\lambda = 0.05$ and $V_C = 40$, 55, 70, 100, 130, and 220 km s^{-1} are indicated with gray filled squares (*left to right*). Model predictions for a ram pressure stripping event at different epochs are indicated by dashed ($\epsilon_0 = 1.2\ M_\odot$ kpc^{-2} yr^{-1}) and dotted ($\epsilon_0 = 0.4\ M_\odot$ kpc^{-2} yr^{-1}) lines, while the starvation scenario is indicated by the long-dashed line. One should take care that the models presented in this figure and later are not evolutionary tracks, but result from the combined effects of ram pressure, recycled gas, and epoch of the interaction. Especially, we note that for interaction that occurred a long time ago, the available gas at that time was smaller (the galaxy was not yet fully formed), and as a result, the final gas amount is also smaller. [*See the electronic edition of the Journal for a color version of this figure*.]

reflects the *n* exponent of the Sérsic law. In practice, it can be used as an indicator of the presence of bulges,[9] thus to quantitatively compare the radial profiles of star-forming and quiescent dwarfs, as shown in Figure 10. For luminosities $L_H \leq 10^{8.4}\ L_{H\odot}$ the quiescent galaxy population is undersampled. In the $10^{8.4}\ L_{H\odot} < L_H \leq 10^9\ L_{H\odot}$ range both galaxy populations are dominated by objects with near-IR concentration indices $C_{31}(H) \leq 3$ (55% and 78% for early and late type, respectively), typical of exponential profiles. The frequency of dwarfs with pronounced central cusps [$C_{31}(H) > 3$] increases with luminosity, with an overall frequency comparable in the quiescent (64%) and star-forming (42%) galaxy populations in the luminosity range $10^9\ L_{H\odot} < L_H \leq 10^{9.6}\ L_{H\odot}$. Values of $C_{31}(H) > 3$ are more frequent in nucleated dEs (*large filled circles*) and in high surface brightness star-forming galaxies (*open squares and crosses*: spirals; *open triangles*: BCDs[10]). We remind that ram pressure stripping events are not expected to deeply modify the relative weight of bulges in perturbed galaxies (Boselli et al. 2006).

For the star-forming galaxies, the *H*-band effective surface brightness and the luminosity are correlated, with a relatively large scatter, with higher disk surface brightnesses in more massive galaxies. The unperturbed models predict a similar correlation, but with a small shift with respect to the observations (which show higher surface brightnesses than model predictions). These discrepancies could be explained by a combination of several effects. First, as we noted above, the models are computed for an average spin, but surface brightness is sensitive to the spin parameter, thus we do expect a large scatter in such a plot. Second, small galaxies may have intrinsic irregularities (linked to sporadic episodes of star formation) affecting the effective surface brightness, which are not included in the models. Finally, the models only consider pure disks, which is the case only at low luminosities. If we make a further separation of the star-forming dwarfs into different morphological classes (see Fig. 11), we can see that the lowest surface brightnesses are reached only by Magellanic irregulars (Sm–Im). The *H*-band effective surface brightnesses of the dEs are similar to those of the star-forming BCDs and spirals (Sa–Sd) of similar luminosity. We notice, however, that the sample of dEs with available near-IR imaging is slightly biased toward high surface brightness, nucleated objects: among the 15 dE galaxies with the lowest values of $\mu_e(B)$, only 20% have a measure of $\mu_e(H)$, while among *B*-band high surface brightness objects 69% have measured $\mu_e(H)$.

The relationship between the *B*-band effective surface brightness and the *H*-band luminosity of dE and Scd–Im–BCD galaxies is significantly dispersed, but consistent with the model predictions. The effective surface brightnesses of quiescent and star-forming systems are more similar in the *B* band than in the *H* band. We notice, however, that dwarf ellipticals have effective surface brightnesses slightly higher than Magellanic irregulars and smaller than late-type spirals and BCDs of similar luminosity. Quiescent systems resulting from the quenching of the star formation activity of Magellanic irregulars, whose existence is predicted by our models, are excluded from our sample just because they have *B*-band surface brightnesses below the detection limit of the VCC.

The variations induced by the interactions are more evident in the UV bands. In the NUV band, for instance, star-forming galaxies (of all types) have ~2–3 mag brighter surface brightnesses than quiescent dwarfs, as predicted by models. The most important variations of the surface brightness of perturbed galaxies predicted by models are in the FUV band (up to 4 mag). The low *GALEX* sensitivity, however, prevents us from detecting most of the dEs that, as expected, have $\mu_e(\mathrm{FUV}) > 26.5$ mag arcsec^{-2}.

We can thus conclude that the observed spectrophotometrical and structural properties of dwarf ellipticals are consistent with those of star-forming dwarfs once their activity has been stopped after a ram pressure gas stripping event able to remove their total gas content. High surface brightness star-forming objects should be the progenitors of the dwarf ellipticals, while Magellanic irregulars should be the progenitors of quiescent objects of low surface brightness not detected in the VCC.

5. THE TRANSITIONAL OBJECTS

The analysis of Figure 7 (see previous section) reveals the existence of several objects having spectrophotometric properties in between that of star-forming late-type galaxies and quiescent spheroidals. The UV selection, which is strongly biased toward star-forming objects, favors the detection of such blue, still active dwarf ellipticals. Figure 12 shows the same FUV − *H* color-magnitude relation given in Figure 7 but using different color symbols (only for early-type galaxies) to indicate still star-forming galaxies (Hα EW$_{\mathrm{em}} > 2$ Å; *red*), poststarburst galaxies that recently ended their activity as indicated by their strong Balmer Hβ absorption line (Hβ EW$_{\mathrm{abs}} > 2.8$ Å; *blue*), H I–detected

[9] The concentration index is, however, insensitive to the presence of small nuclei such as those present in nucleated Virgo Cluster dEs.

[10] We included in this category also the mixed classes S/BCD, Sm/BCD, and Im/BCD.

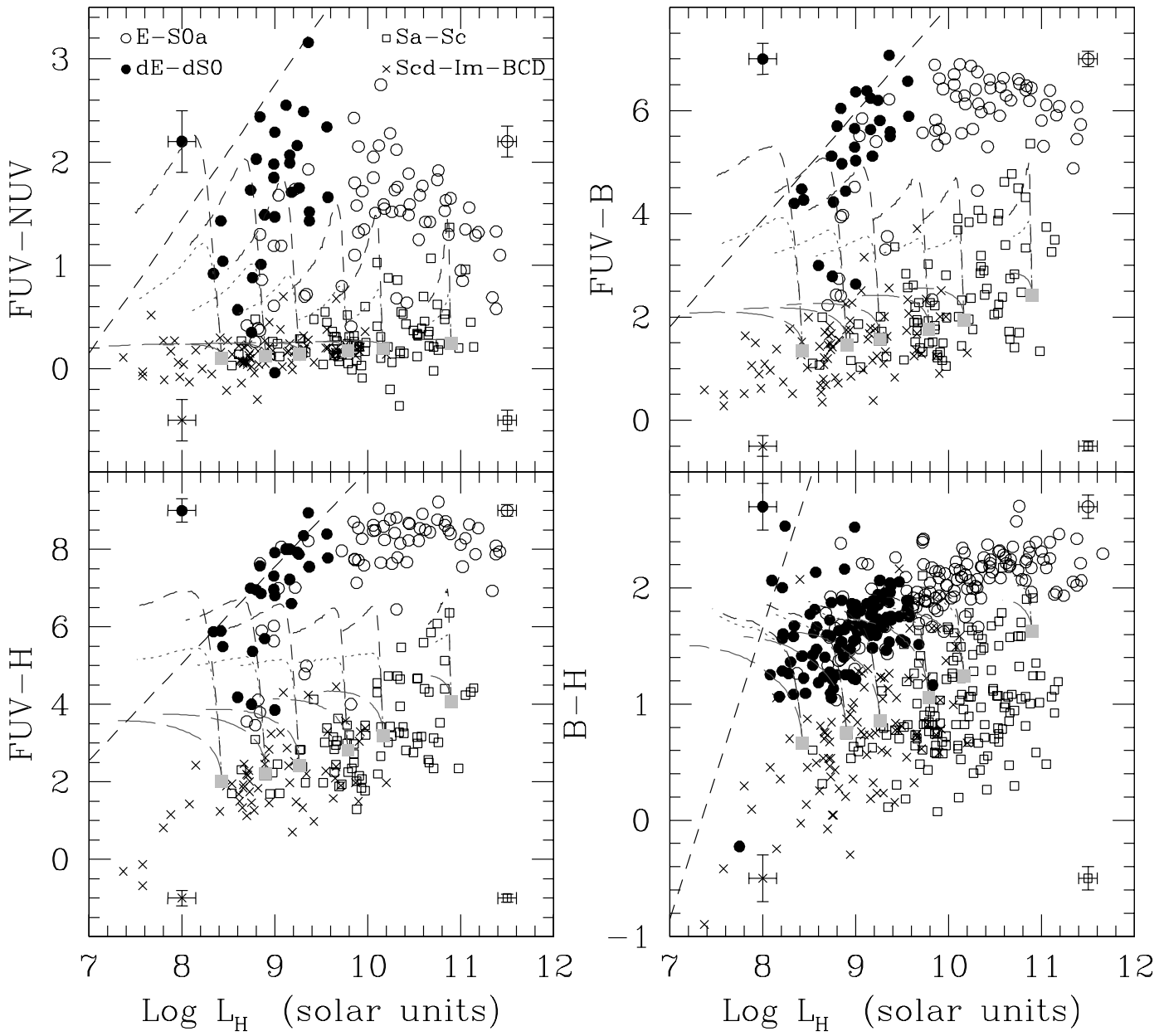

FIG. 7.— Relationships between different UV, optical, and near-IR color indices and the *H*-band luminosity compared to model predictions. Symbols and models are as in Fig. 6. Galaxies redder than the dashed line are undetectable by the present surveys. [*See the electronic edition of the Journal for a color version of this figure.*]

objects (*green*), and rotationally supported spheroidals ($v^*/\sigma > 0.5$; *magenta*).[11]

We can photometrically define the transitional class as being formed by those objects of luminosity $\log L_H < 9.6\ L_{H\odot}$ with $3 < \mathrm{FUV} - H < 6$. The early-type galaxies in our sample satisfying this criterion are listed in Table 2.

5.1. *The UV to Near-IR Spectral Energy Distribution*

Figure 12 and Table 2 clearly show that most of the low-luminosity early-type galaxies with blue colors are characterized by an ongoing or recent star formation activity (strong emission or absorption Balmer lines; see Fig. 15 below). Two of them have been detected in H I, while none have rotational velocity measurements.

Figure 13 shows how the UV to near-IR SED of a star-forming dwarf galaxy of $\lambda = 0.05$ and rotational velocity $V_C = 55\ \mathrm{km\ s^{-1}}$ changes with time after a ram pressure stripping event characterized by an efficiency $\epsilon_0 = 1.2\ M_\odot\ \mathrm{kpc^{-2}\ yr^{-1}}$. For comparison the model SEDs are plotted along with the observed SED of the BCD galaxy VCC 24 and the dwarf ellipticals M32 and NGC 205.[12] The SED of an unperturbed galaxy is similar to that of star-forming dwarf systems such as the BCD VCC 24, while it becomes redder soon after the interaction, reaching the values of the dwarf elliptical NGC 205 after 1.3 Gyr. Two interactions are

[11] The anisotropy parameter v^*/σ is defined as $v^*/\sigma = (v/\sigma)/[e/(1-e)]^{1/2}$, where e is the ellipticity of the galaxy.

[12] We compare the prediction of our model to the SED of NGC 205 and M32 just because these two objects are the only well-known dwarf ellipticals detected by *GALEX* in the two filters. We remind, however, that NGC 205 is a nonstandard dE with central gas and some star formation activity that would make it classified as a dE with blue center by Lisker et al. (2006a). Given its high surface brightness, M32 is a nongenuine dwarf elliptical. The photometric data of NGC 205 and M32 are taken from Gil de Paz et al. (2007).

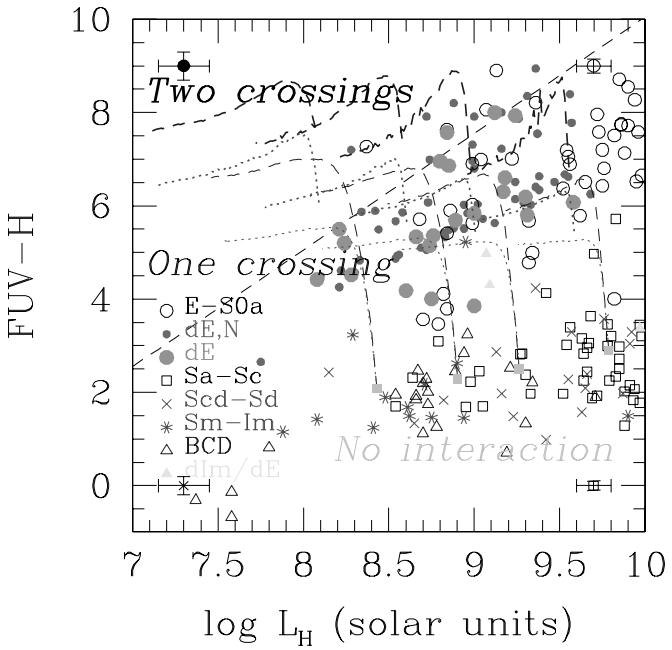

FIG. 8.—Relationships between the FUV − *H* color index and the *H*-band luminosity of dwarf galaxies compared to model predictions in the case of single (*thin lines*) or multiple (*thick lines*) interactions. *Open squares*: Sa–Sc; *crosses*: Scd–Sd; *asterisks*: Sm–Im; *open triangles*: BCD; *filled triangles*: dIm/dE; *open circles*: E–S0a; *small filled circles*: nucleated dEs; *large filled circles*: nonnucleated dEs. Models are for galaxies of spin parameter $\lambda = 0.05$ and rotational velocity $V_C = 40$, 55, 70, and 100 km s^{-1} from left to right, respectively. Galaxies redder than the dashed line are undetectable by the present surveys. [*See the electronic edition of the Journal for a color version of this figure*.]

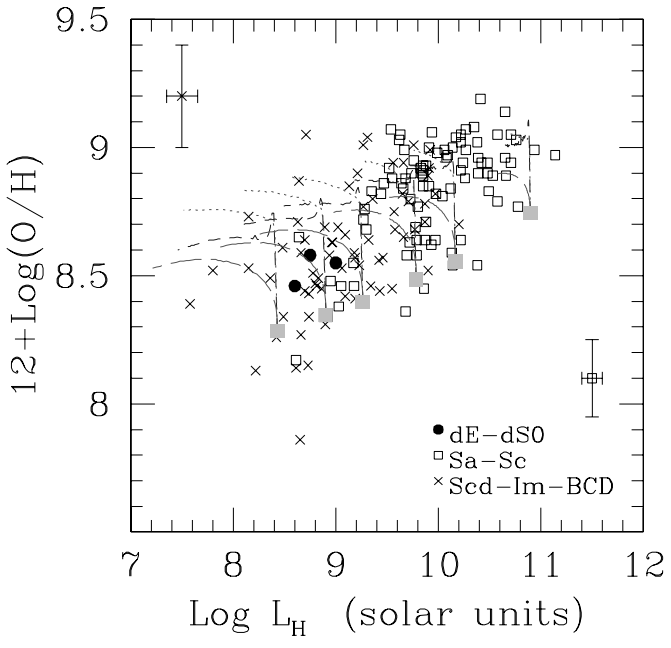

FIG. 9.—Relationships between the gas 12 + log (O/H) metallicity index and the model predictions. Symbols and models are as in Fig. 6. The three dE galaxies in the plot are the transitional types VCC 710 [12 + log (O/H) = 8.55], VCC 1501 [12 + log (O/H) = 8.46], and VCC 1617 [12 + log (O/H) = 8.58]. [*See the electronic edition of the Journal for a color version of this figure*.]

necessary to get colors as red as those of the compact dwarf elliptical M32.

During the transition phase, the FUV − *H* color gets redder while the *H*-band magnitude is slightly reduced with respect to the reference case (Fig. 14). We can use these properties to estimate the rotational velocity and look-back time to the interaction. All the galaxies are close to the 40–55–70 km s^{-1} range for which we computed models. We thus interpolated (and extrapolated above 70 km s^{-1}) in 1 km s^{-1} bins our models. Figure 14 shows the position of each of these models (for the 1.2 $M_\odot$ kpc^{-2} efficiency) in the FUV − *H* versus log L_H diagram. The models at the bottom of the diagram are unperturbed. Each point along the lines for different velocities corresponds to various values of the stripping look-back time ($t_{rp} = 0$, 0.1, 0.2, 0.3,. . .). Velocities and look-back times for each transitional object can easily be found by a simple least-squares test (see Table 2 and Fig. 15). Models indicate that all transitional objects recently (<650 Myr) interacted with the cluster IGM.

5.2. *Color Gradients*

It has been shown that some dwarf elliptical galaxies have inverted color gradients, with bluer colors in the center (Lisker et al. 2006a and references therein). Indeed, 6 out of the 16 galaxies listed in Table 2 have been defined as "blue center" by Lisker et al. (2006a).

The observed inversion of the color gradient in the center of dwarf galaxies is obtained in our multizone models in a ram pressure stripping scenario (see Fig. 16) for recent interaction of relatively weak efficiency (0.1 $M_\odot$ kpc^{-2}), and has the same origin as that observed in massive spirals such as NGC 4569 (Boselli et al. 2006). Blue colors in the center of these dwarf galaxies are expected because ram pressure stripping is more efficient in the outer disk, where all the gas is removed, while some gas needed to feed star formation might be retained in the central part where the galaxy potential is deeper. For more efficient interactions, the contribution of the recycled gas becomes important whenever the interaction started long ago in the center of galaxies, where the stellar surface density is high and we obtain again blue centers. We should note that if galaxies have deep potential wells because of a central mass condensation (not taken into account in our models), the gas in the center should be harder to remove, easily making blue cores. Given the shape of the potential well, whose deepness increases with mass (Catinella et al. 2006), we expect that the inversion of the color gradient is more frequent and radially extended in the brightest dwarfs, which are more likely to retain some gas, as indeed observed (Lisker et al. 2006a). The look-back time to the ram pressure stripping event, combined with the age of the different stellar populations sampled in the various filters, makes the observed color inversion more pronounced at short wavelengths, as shown in Figure 16. We can also add that such an inversion of the color gradient cannot be reproduced in a starvation scenario where gas removal is not a radial but rather a global effect.

For those galaxies with available SDSS images we reconstructed their NUV − *i* color gradient (see Fig. 15) using SDSS images smoothed to the *GALEX* resolution. Twelve out of the 14 galaxies with available data have indeed blue colors in their center (Fig. 15 and Table 2), as expected if these galaxies recently underwent a ram pressure stripping event. We remark that the observed blueing of the inner gradient happens in the inner 1–2 kpc, as predicted by models (Fig. 16).

Seven of the transitional class galaxies (VCC 327, VCC 450, VCC 597, VCC 710, VCC 1175, VCC 1617, and VCC 1855) have been imaged in Hα with the San Pedro Martir 2 m telescope (Gavazzi et al. 2006a). All galaxies (except VCC 327, undetected in Hα imaging) show a similar pattern, with the star formation activity always limited to the central region and not extended to

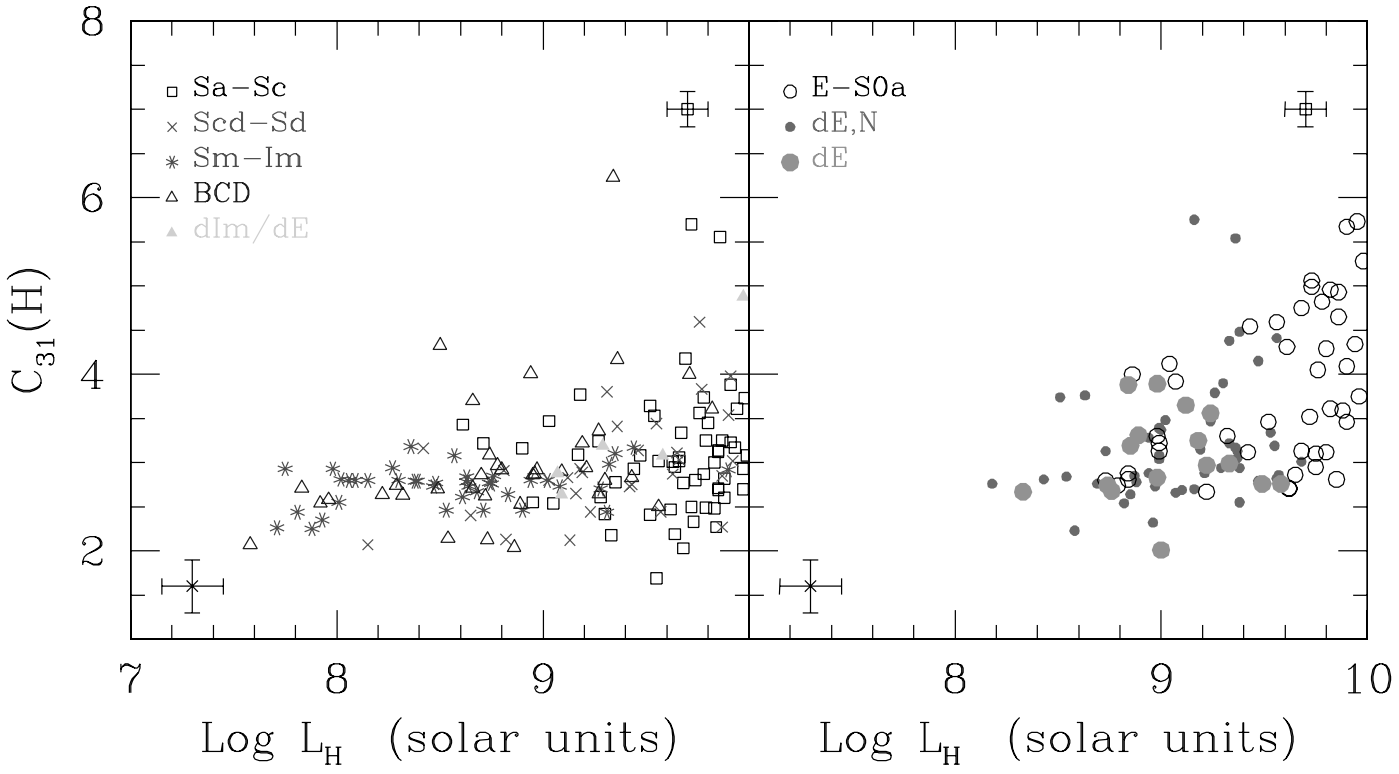

FIG. 10.—Relationship between the H-band $C_{31}(H)$ parameter and the H-band luminosity for early- (*right*) and late-type (*left*) galaxies with $L_H < 10^{10}\ L_{H\odot}$. Symbols are as in Fig. 8. [*See the electronic edition of the Journal for a color version of this figure.*]

the whole disk, once again as predicted by our model, as shown in Figure 17 for VCC 710.

6. DISCUSSION

The analysis done so far clearly indicates that some dwarf ellipticals might result from the rapid decrease of the star formation activity of low-luminosity, late-type galaxies after most of their gas was lost because of their strong interaction with the hostile cluster environment. The comparison between model predictions and observations favors ram pressure stripping events with respect to galaxy starvation. Models in fact predict that low-luminosity spirals, Im dwarfs, and BCDs suffering starvation since 6 Gyr are still star-forming galaxies with blue UV colors, relatively strong Balmer emission lines (Hα $EW_{em} \sim 10$ Å), and have an H I gas content ($\sim 10^8\ M_\odot$) easily detectable by H I surveys such as ALFALFA and AGES. These objects would thus still be classified as star-forming dwarf galaxies, and not dwarf ellipticals.

We should first notice that our simple representation of a ram pressure stripping event is totally consistent with the high-resolution hydrodynamical simulations in cluster dwarf galaxies of Mori & Burkert (2000), Murakami & Babul (1999), and Marcolini et al. (2003), which predict the stripping of the whole gas reservoir on short timescales.

6.1. *Is the Ram Pressure Scenario Consistent with All Observational Evidences?*

As mentioned in § 1, however, several observational evidences, namely, (1) the different structural properties of Magellanic irregulars and dwarf ellipticals, (2) the presence of nuclei in dEs, (3) the higher specific frequency of globular clusters and (4) the higher stellar metallicity of quiescent systems with respect to star-forming dwarfs, (5) their different velocity distribution, and (6) the different shape of the field and cluster luminosity functions, have been often indicated as major limitations to the formation of cluster dwarf ellipticals through the gas stripping of star-forming systems. We see in this section how these difficulties can be overcome.

6.1.1. *Structural Properties*

In general, we can say that the present work gives a natural explication to the presence of rotationally supported (Pedraz et al. 2002; Geha et al. 2003; van Zee et al. 2004b), gas-rich (Conselice et al. 2003b; van Zee et al. 2004b), star-forming dwarf ellipticals. The presence in some dwarf ellipticals of spiral arms observed by Lisker et al. (2006b) is further evidence of the rotating/spiral origin of these objects. The grand-design spiral arms of these dEs, apparently different from the flocculent open arms of very late type spirals, might be driven by disk instabilities produced by the displacement of the gas over the stellar disk during the stripping event (Elmegreen et al. 2002). Consistently with observations, which have shown that the frequency of dEs with grand-design spiral arms increases with luminosity (Lisker et al. 2006b), the perturbations induced by the gas displacement are expected to be important only in those objects where the potential is sufficient to retain some gas, while totally absent in the lowest luminosity systems where the whole gas content is instantaneously removed.

The comparison of model predictions with observations suggests that on average the variation of the structural parameters (surface brightnesses, effective radii, and concentration indices) of high surface brightness, low-luminosity, star-forming galaxies such as BCDs or late-type spirals (mostly Scd–Sd) at various wavelengths expected after a ram pressure stripping event might indeed reach the values observed in dEs. Consistently with Bothun et al. (1986), we confirm that the sampled dEs have near-IR and optical surface brightnesses higher than those of Magellanic

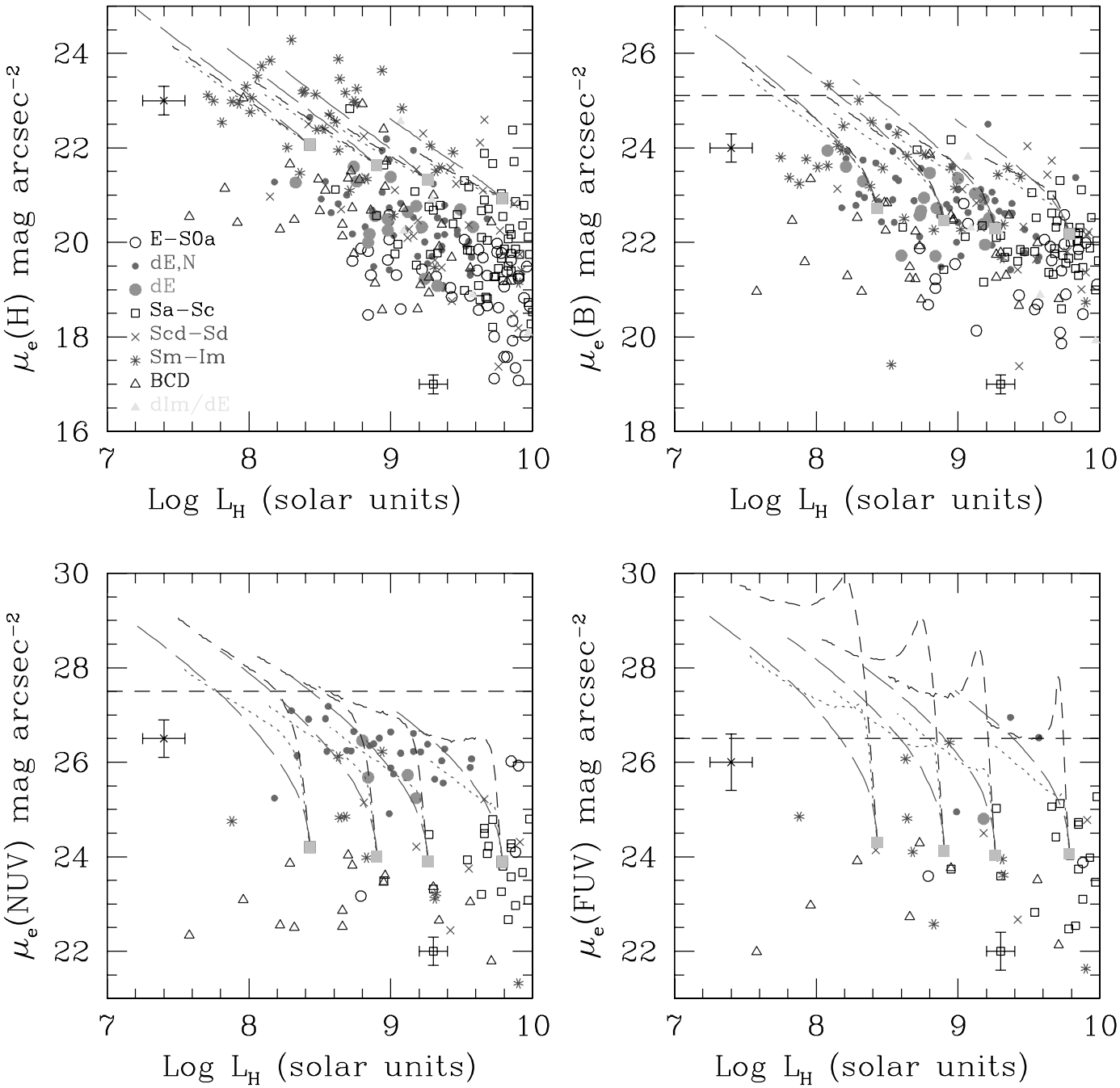

FIG. 11.— Relationships between the *H*, *B*, NUV, and FUV effective surface brightnesses (in AB magnitudes) and the *H*-band luminosity. Symbols and models are as in Fig. 8. The horizontal dashed lines in the *B*, NUV, and FUV panels are the surface brightness detection limits of the VCC and *GALEX*. [*See the electronic edition of the Journal for a color version of this figure*.]

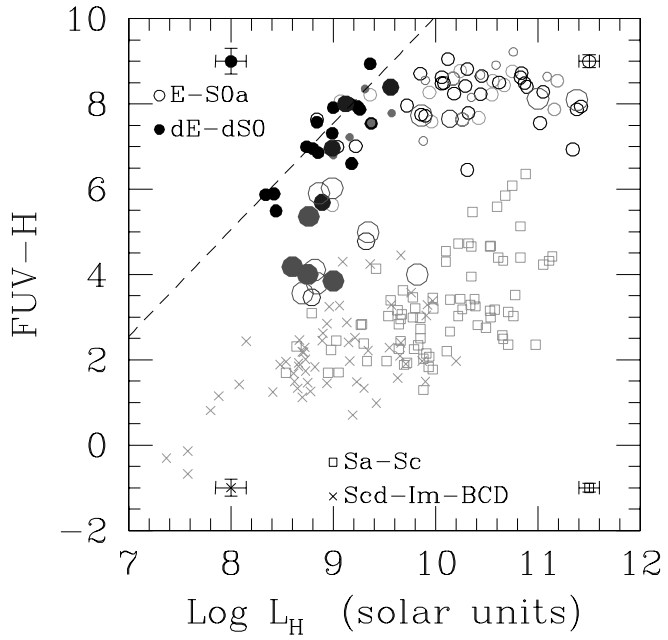

FIG. 12.—Relationship between the FUV − H color index and the H-band luminosity (see Fig. 7). Early-type galaxies (*filled circles*: dE–dS0; *open circles*: E–S0–S0a) are coded as follows: large symbols are for galaxies with Hα emission (Hα EW$_{em}$ > 2 Å), medium large symbols for objects with strong Hβ absorption lines (Hβ EW$_{abs}$ > 2.8 Å), medium small symbols for H I–detected galaxies, small symbols for rotationally supported galaxies ($v^*/\sigma > 0.5$), and black symbols for galaxies with spectroscopy but not satisfying the previous criteria. Colors are mutually exclusives, with priority ordered according first to the Hα emission, then to the Hβ absorption, to the H I detection, and to rotationally supported objects. Gray symbols are for the whole late-type galaxy population and for early-type objects without any spectroscopic information. [*See the electronic edition of the Journal for a color version of this figure*.]

irregulars (Sm–Im) and thus cannot result from this galaxy population. Our models, however, predict the existence in the Virgo Cluster of an extremely low surface brightness quiescent galaxy population [$\mu_e(B) \geq 25$ mag arcsec^{-2}] resulting from the quenching of the star formation activity of Magellanic irregulars. Such a population has been indeed observed by Sabatini et al. (2005).

Our model predictions cannot be easily compared to the results of Lisker et al. (2006a, 2006b, 2007) and Binggeli & Popescu (1995) on the flattening distribution of star-forming and quiescent dwarfs since models do not take into account the three-dimensional evolution of the disks. We can argue that the lack of supply of young stars with low velocity dispersion because of the suppression of the star formation activity causes the disk to heat up, dumping spiral waves on timescales of a few revolutions (Sellwood & Carlberg 1984; Fuchs & von Linden 1998; Elmegreen et al. 2002), in particular in low-luminosity systems where the rotational component is not always dominant. In low-luminosity rotating systems (70–130 km s^{-1}) it has been observed that the disk scale height increases by a factor of ~2 in ~3 Gyr (Seth et al. 2005). We could thus expect that the flattening distribution is age dependent. In the lack of external gravitational perturbations, the rotational velocity is conserved while σ increases once the gas is removed. Gravitational perturbations induced by the interaction with other galaxies or with the cluster potential would heat up the system and disperse the angular momentum, thus speeding up the decrease of v/σ (H. Wozniak 2007, private communication). We would thus expect rounder shapes and more relaxed distributions in those objects where the star formation stopped long ago. We remark that, although still not virialized, nucleated objects are more centrally clustered than nonnucleated systems (Lisker et al. 2007).

6.1.2. *Nuclearity*

The angular resolution of our model is too poor (~1 kpc) to make any prediction on the formation process and evolution of

TABLE 2
THE TRANSITIONAL CLASS

VCC (1)	Type (2)	Blue Centers (3)	log ($L_H/L_{H\odot}$) (4)	FUV − H (mag) (5)	Hα EW$_{em}$ Emission (Å) (6)	Hβ EW$_{abs}$ Absorption (Å) (7)	log ($M_{H\,I}/M_\odot$) (8)	Age ($\epsilon_0 = 1.2$) (Gyr) (9)	V_C ($\epsilon_0 = 1.2$) (km s^{-1}) (10)
21.....	dS0	bc, BC	8.89	5.69	...	4.2	<7.84	0.50	59
327.....	S0	BC	9.34	4.99	0 (16)	1.1	...	0.22	76
450.....	S0 pec	BC	8.86	5.90	10 (52)	...	...	0.58	58
597.....	S0	BC	8.84	3.79	7 (36)	...	...	0.04	54
710.....	dS0:	1	9.00	3.85	15	...	7.95	0.04	61
764.....	S0	1	8.99	5.63	...	...	...	0.46	63
1065.....	dE0, N	...	8.34	5.87	...	0.8	...	0.64	42
1175.....	E5/S0	bc, BC	8.82	4.11	4 (157)	...	...	0.09	54
1389.....	dE2:, N	...	8.44	5.49	...	1.9	...	0.50	44
1499.....	E3 pec or S0	bc, BC	8.79	3.46	...	5.0	...	0.00	52
1501.....	dS0?	bc, BC	8.60	4.18	4	1.1	...	0.12	47
1539.....	dE0, N	BC	8.42	5.89	...	1.6	...	0.64	44
1617.....	d:S0 pec?	bc, BC	8.75	4.00	9 (7)	1.0	...	0.08	52
1684.....	dS0:	bc, BC	8.76	5.36	(4)	4.5	...	0.41	54
1809.....	S0/Sa	BC	9.32	4.78	...	4.9	7.25	0.18	75
1855.....	S0:	BC	8.70	3.56	20 (72)	...	...	0.01	50

NOTES.—Col. (1): VCC name, from the Virgo Cluster Catalogue of Binggeli et al. (1985). Col. (2): Morphological classification, from Binggeli et al. (1985). Col. (3): Presence of a blue center in $g - i$ from Lisker et al. (2006a) (bc) and/or NUV − i from this work (BC); "1" stands for galaxies not observed by the SDSS. Col. (4): H-band luminosity, in solar units. Col. (5): FUV − H color index, in AB magnitudes. Col. (6): Equivalent width of the Hα emission line, from (in order of preference) imaging (Gavazzi et al. 2006a) and integrated spectroscopy (Gavazzi et al. 2004). Nuclear (SDSS, DR5) spectroscopic data are given in parentheses. Col. (7): Equivalent width of Hβ underlying absorption line, from (in order of preference) integrated (Gavazzi et al. 2004) or nuclear (SDSS, DR5) spectroscopy. Col. (8): Logarithm of the H I mass, in solar units, from Gavazzi et al. (2005a). Cols. (9) and (10): Look-back time to the interaction and rotational velocity of the best-fitting model for a ram pressure stripping event with $\epsilon_0 = 1.2\ M_\odot$ kpc^{-2} yr^{-1}. Look-back times of 0 Myr are for galaxies now at the peak (maximum) of their interaction.

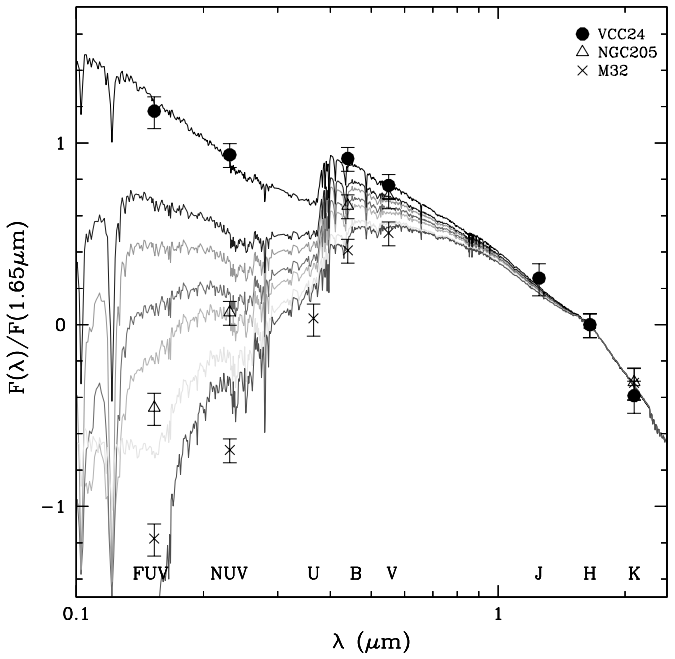

FIG. 13.—UV to near-IR SEDs of the BCD VCC 24 (*filled circles*), the dE NGC 205 (*open triangles*), and the compact dwarf elliptical M32 (*crosses*) (all normalized to the 1.65 μm *H*-band flux) compared to the model SED for a galaxy of spin parameter $\lambda = 0.05$ and rotational velocity $V_C = 55$ km s^{-1}. The black solid line (upper model) is the model for an unperturbed galaxy; the models with decreasing intensity are for galaxies that had their peak of the interaction, respectively, 0, 100, 300, 500, and 1300 Myr and two cluster crossings with the last one 500 Myr ago. [*See the electronic edition of the Journal for a color version of this figure.*]

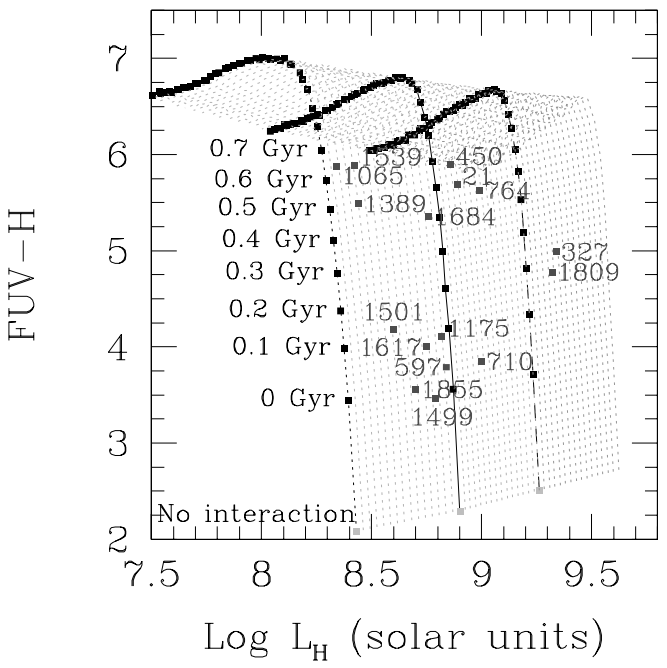

FIG. 14.—Transition objects shown in the FUV − *H* vs. *H*-band luminosity plane. The lines indicate the position of various ram pressure stripping models ($\epsilon_0 = 1.2\ M_\odot$ kpc^{-2} yr^{-1}) interpolated between 40 and 70 km s^{-1} (and extrapolated beyond) without interaction (*squares*), and for various look-back times to the interaction (a few are indicated on the left). These models were used to fit a velocity and look-back time for each transition object. [*See the electronic edition of the Journal for a color version of this figure.*]

the nuclei observed in dwarf ellipticals. As a general remark, we can say that recent *HST* ACS high-resolution observations of nuclei of early-type galaxies in the Virgo Cluster revealed that they have statistical (frequencies) and physical (sizes, luminosities, colors) properties similar to those of the nuclear stellar clusters found in late-type galaxies (Côté et al. 2006), consistently with our evolutionary picture. *HST* observations of dEs show color gradients getting bluer toward their nuclei witnessing a younger stellar population than that of the outer disk (Lotz et al. 2004; Côté et al. 2006). Furthermore, the presence of a nucleus is more frequent in massive dEs than in low-luminosity objects (Sandage et al. 1985; Ferguson & Binggeli 1994).[13]

6.1.3. *Specific Frequency of Globular Clusters*

The rapid evolution expected after the galaxy-ICM interaction that abruptly stops the star formation is able to change the total luminosity of the perturbed galaxy. The typical progenitor of a given dwarf elliptical that did not undergo such a violent truncation of its star-forming activity today would be much brighter than its potential progeny even in the near-IR (see, for instance, Fig. 7). If we make the reasonable assumption that globular clusters were formed in the early phase of galaxy formation (thus well before any possible recent ram pressure stripping event) and regulated by the primordial dark matter condensation, the specific frequency of globular clusters should thus be determined by normalizing the total number of globular clusters to the absolute magnitude of the unperturbed galaxy, which is always brighter than its gas-stripped counterpart. With the specific frequency of globular clusters defined as $S_N = N_{\rm GC} \times 10^{0.4(M_V+15)}$ (where $N_{\rm GC}$ is the number of globular clusters; Strader et al. 2006), we can see that S_N increases with time after a ram pressure stripping event just because the absolute magnitude M_V of the perturbed system does not increase with time as that of its unperturbed counterpart (see Fig. 18). The specific frequency of globular clusters in dE galaxies ranges in between $\sim$1 and $\sim$20 with roughly a double distribution peaked at $S_N \sim 2$ and $\sim$10 (Strader et al. 2006). These values are consistent with a scenario where dEs have been formed through a ram pressure gas stripping event of low-luminosity late-type galaxies (whose specific frequency is $S_N \leq 1$; Miller et al. 1998) and occurred $\leq$4 Gyr ($\leq$1 Gyr for dEs with $S_N \sim 2$).

6.1.4. *Metallicity*

Grebel et al. (2003) observed an increase of the metallicity measured in the old stellar populations in dwarf spheroidals with respect to dwarf irregulars of similar luminosity. It is equivalent to say that the spheroidals are fainter than irregulars for the same stellar metallicity. This is naturally obtained in our models: let us consider a "common ancestor," giving rise to a low-luminosity, star-forming galaxy if it evolves in isolation and to a dE if its star formation activity is suppressed after an interaction. The metallicity in the old population will be the same (the one of the common ancestor). The luminosity of the star-forming object will be the one of the unperturbed model, while the one of the quiescent system will be the one of the model after an interaction. Figure 18 shows that the difference in *V*-band luminosity (partly due to the fading of the stellar population, but also to the fact that less stars formed in the latter than in the former case) is of $\sim$1 mag after 1 Gyr. This luminosity difference for the same metallicity corresponds well

[13] High-resolution *HST* observations of dwarf ellipticals in the Virgo Cluster revealed the presence of small nuclei also in objects classified as nonnucleated in the VCC (Lotz et al. 2004; Côté et al. 2006), whose distribution does not seem to depend on the position within the Virgo Cluster. For consistency with our morphological classification and for completeness reasons, we consider here the VCC classification, which might be biased, for its limited angular resolution, to the most extended nuclei.

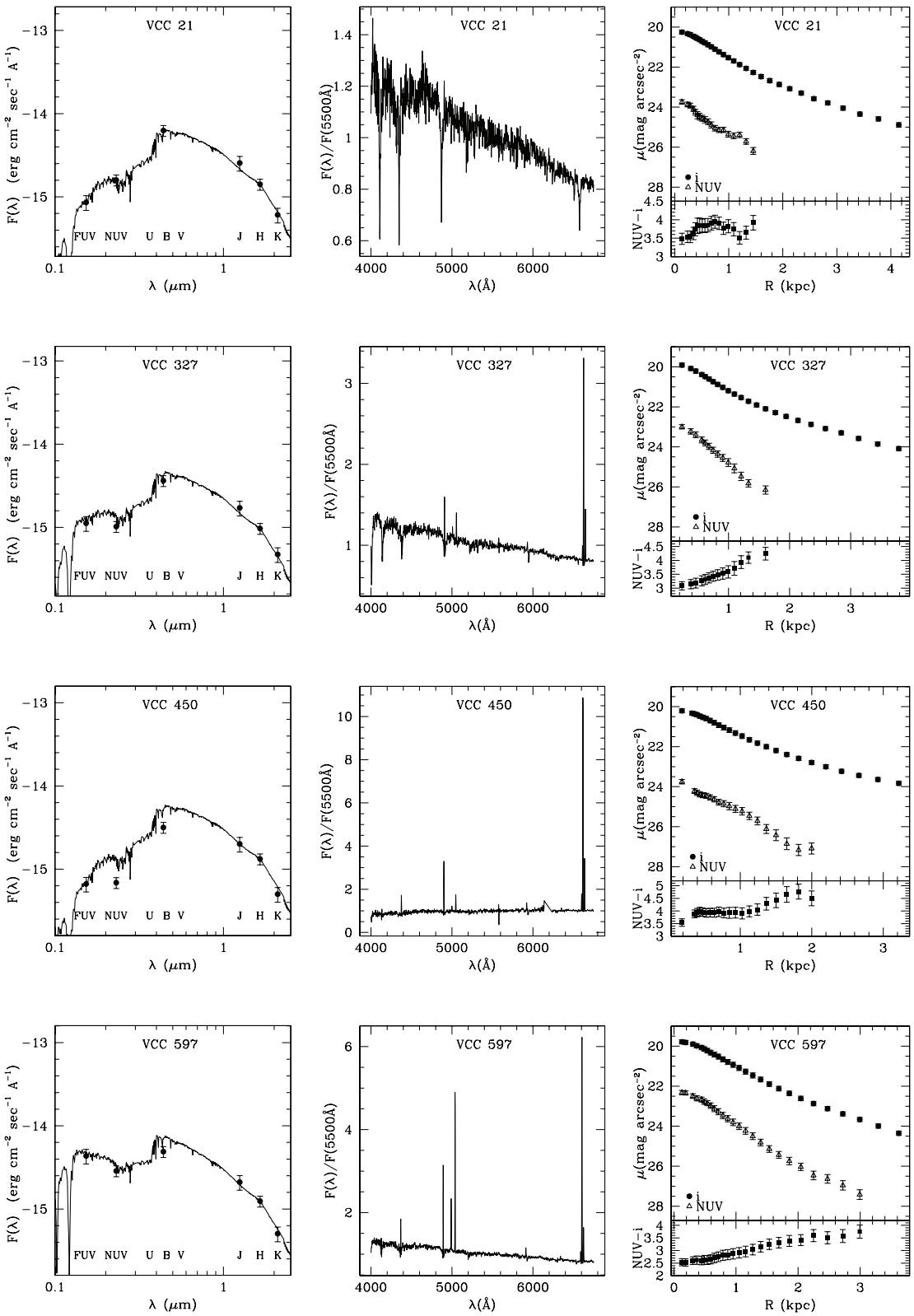

FIG. 15.—*Left*: Observed (*filled circles*) and model-predicted (*solid line*) SED of the transitional galaxies listed in Table 2 in a ram pressure stripping scenario with $\epsilon_0 = 1.2\,M_\odot\,\mathrm{kpc}^{-2}\,\mathrm{yr}^{-1}$. The look-back time to the interaction and the rotational velocity of the galaxy for the model SED are listed in Table 2. *Middle*: Integrated (from GOLDMine) or nuclear (from SDSS) visible spectrum. Only integrated spectra have been used in the construction of the UV to near-IR SED shown in the left column. *Right*: NUV − *i* radial profiles (in AB magnitudes).

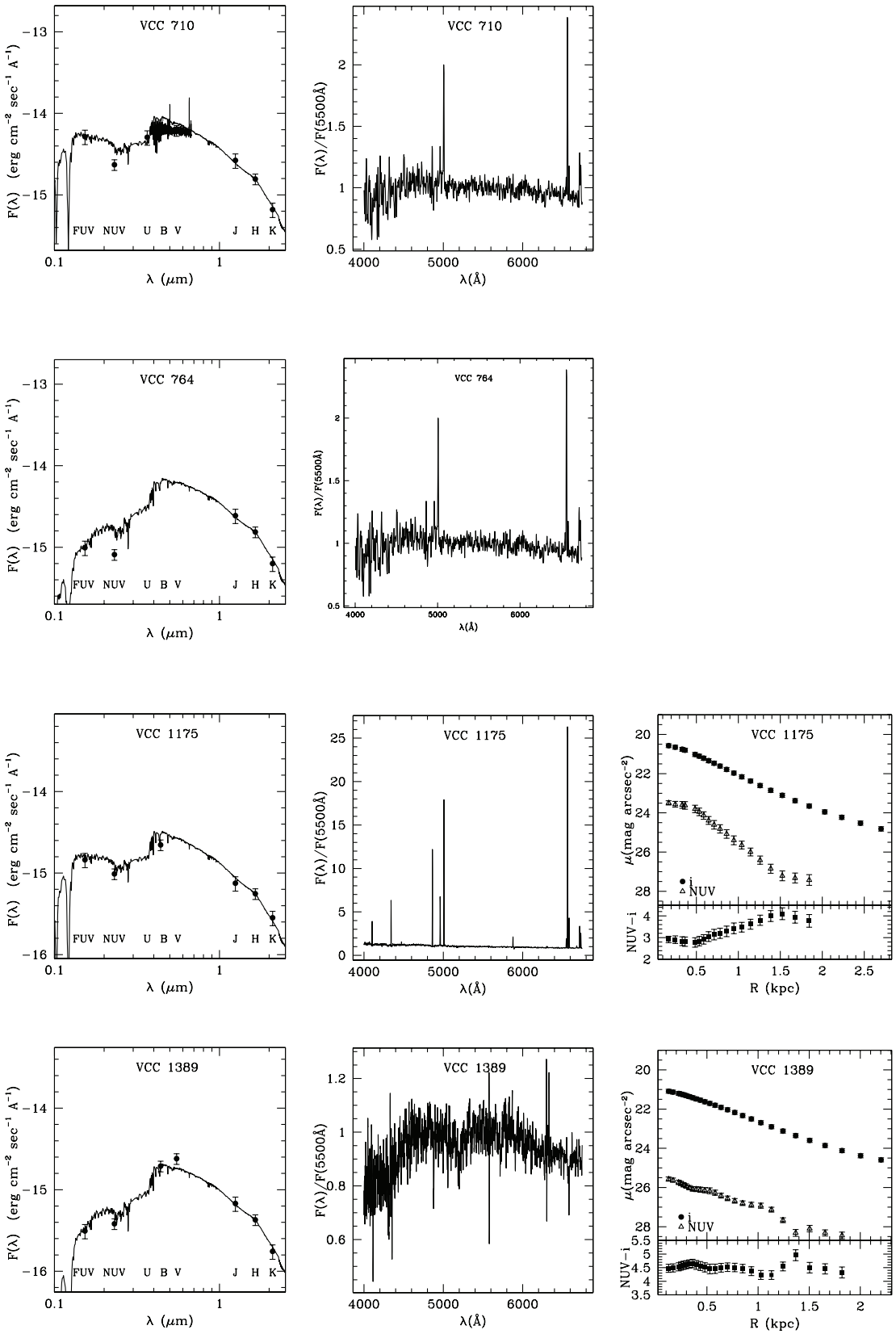

FIG. 15—*Continued*

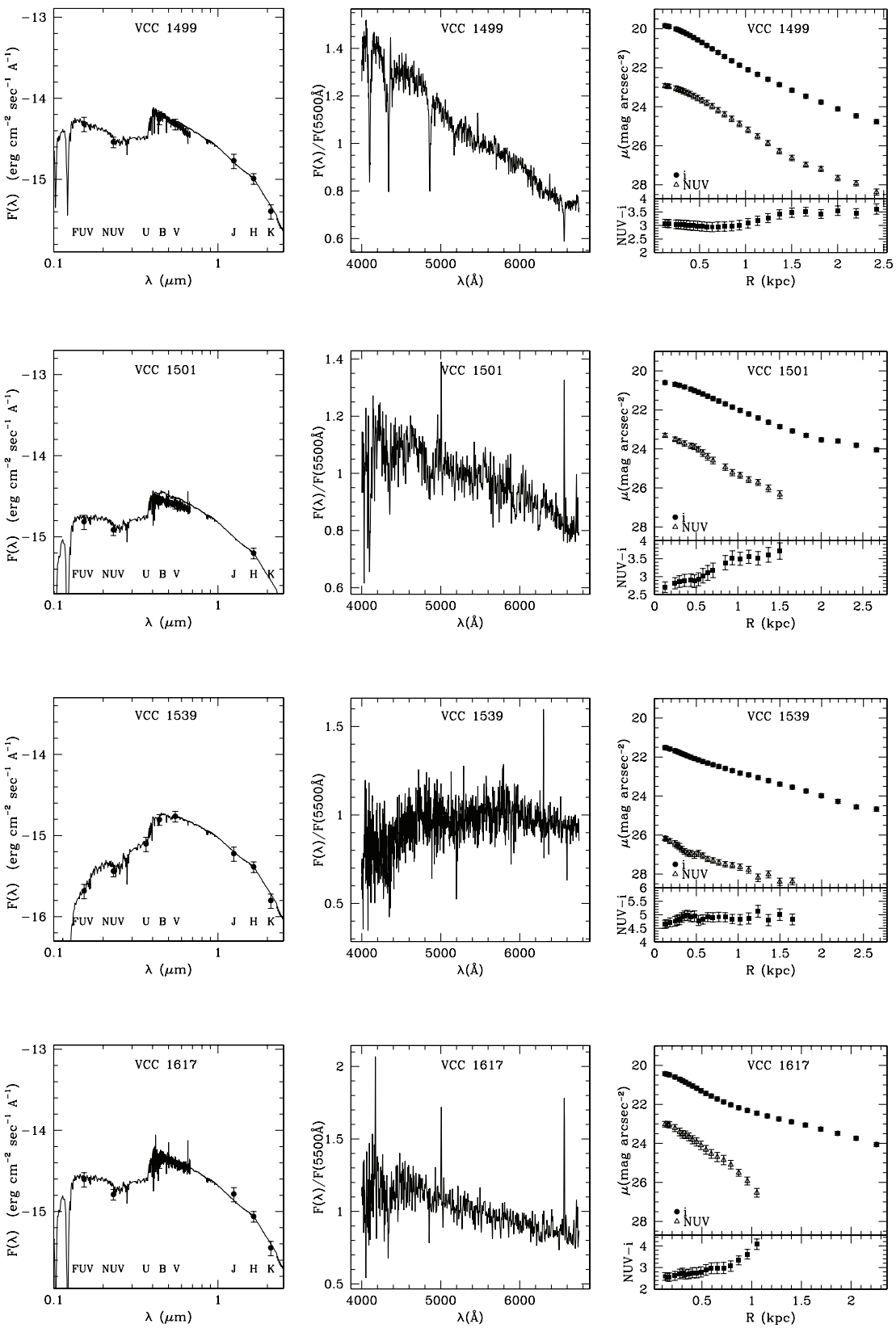

FIG. 15—*Continued*

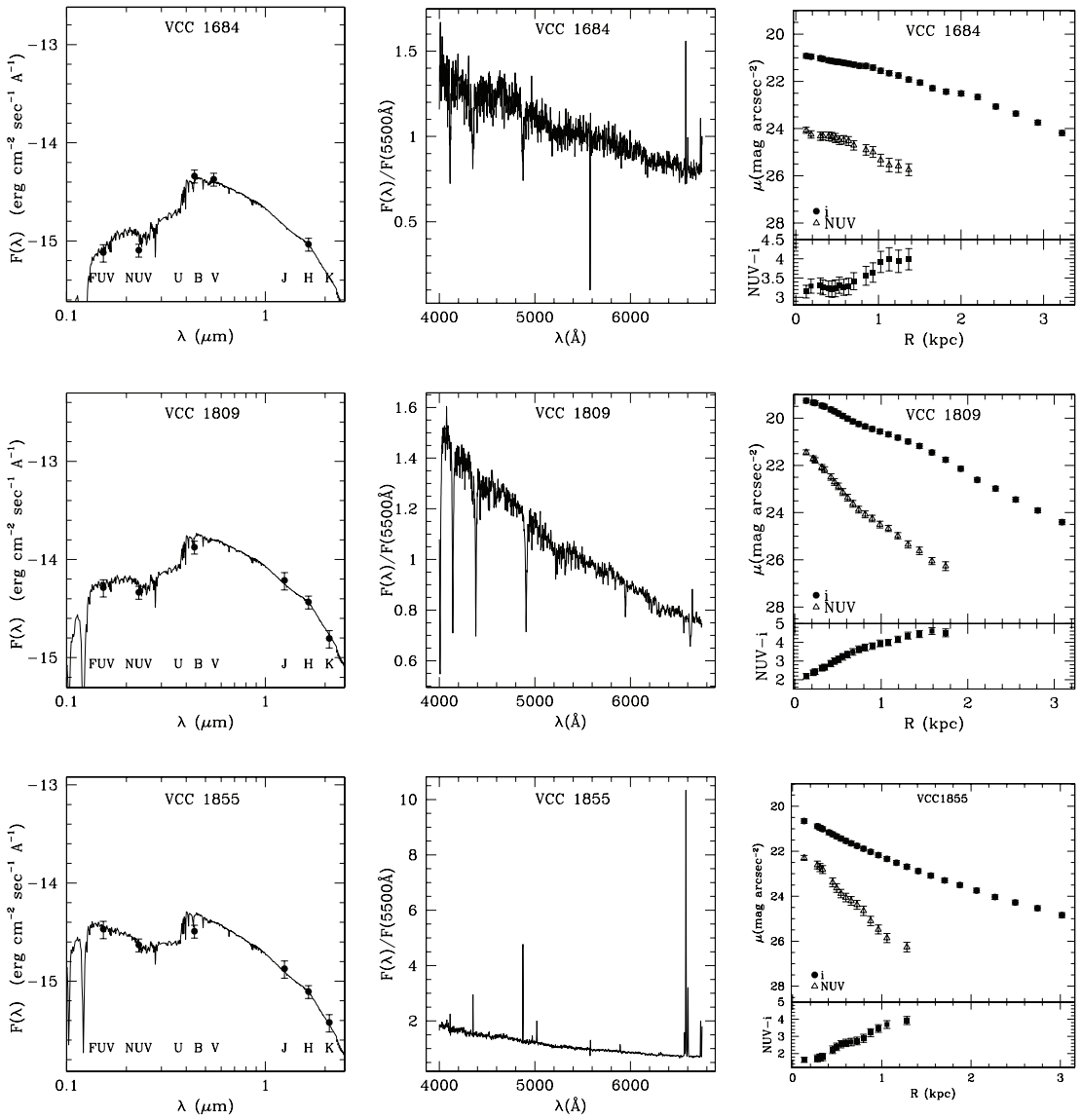

FIG. 15—*Continued*

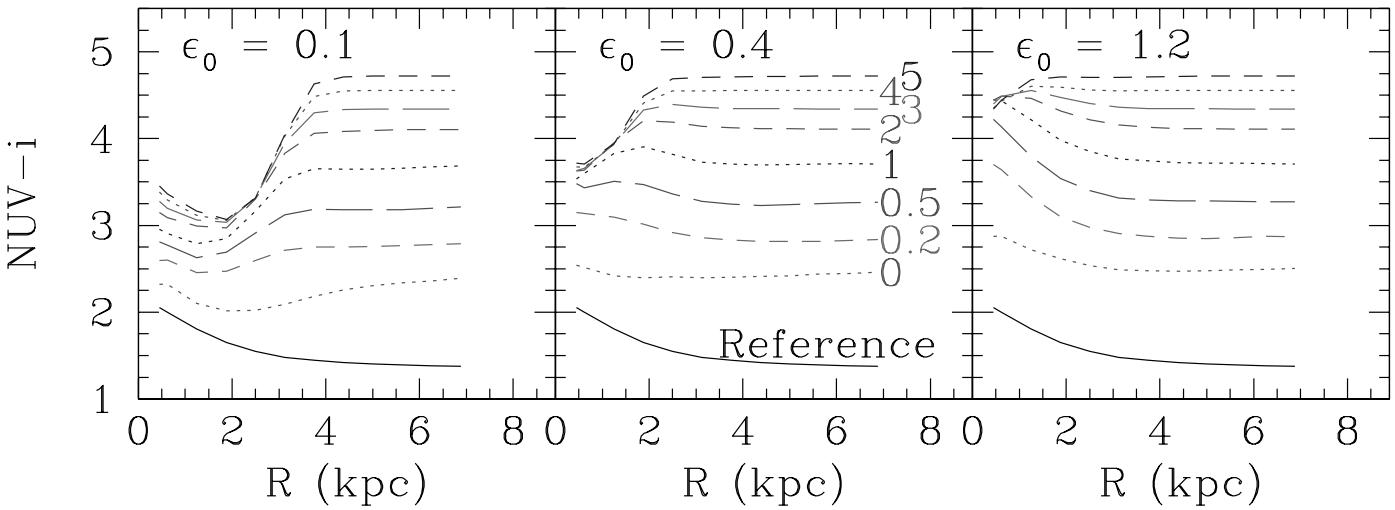

FIG. 16.— Variation of the NUV − *i* color radial profile (in AB magnitudes) with time for a galaxy with rotational velocity $V_C = 55$ km s^{-1} and spin parameter $\lambda = 0.05$ after a ram pressure stripping event with efficiencies $\epsilon_0 = 0.1$ (*left*), 0.4 (*middle*), and 1.2 $M_\odot$ kpc^{-2} yr^{-1} (*right*). The look-back time to the interaction in Gyr is indicated on the right in the middle panel, from 0 (epoch when the interaction is at its maximum; *dotted line*) to 5 Gyr (*dashed line*); the solid line is the reference unperturbed model. [*See the electronic edition of the Journal for a color version of this figure*.]

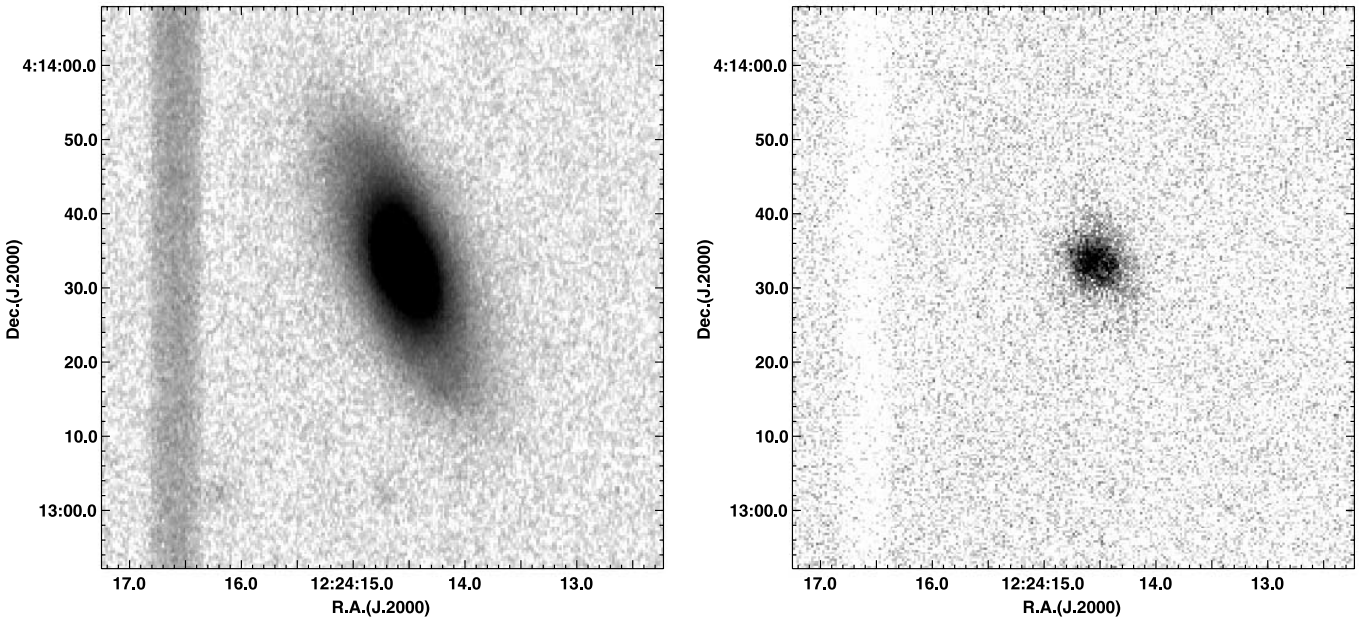

FIG. 17.—Red stellar continuum (*left*) and the Hα+[N II] narrowband images (*right*) of the dS0 galaxy VCC 710 from our own observations.

to that observed by Grebel et al. (2003) between the star-forming and quiescent dwarf galaxy populations.

6.1.5. *Velocity Distribution*

The velocity distribution of the low-luminosity ($L_H < 10^{10}\ L_{H\odot}$), high surface brightness [$\mu_e(H) < 22$ mag arcsec^{-2}], star-forming galaxies (see Table 3), i.e., of those objects that our models indicate as the probable progenitors of the observed dwarf ellipticals, is strongly non-Gaussian, with a pronounced wing at high velocity (see Fig. 19), witnessing infall. If limited to the Virgo A subcluster, thus to the region associated to the hot gas emitting in X-ray where ram pressure is active (Gavazzi et al. 1999), the probability that both nucleated and nonnucleated dwarf ellipticals are driven by the same parent population as low-luminosity, high surface brightness, star-forming galaxies is relatively important ($P \sim 40\%$), as indicated by Kolmogorov-Smirnov tests (see Table 4). Although dynamical considerations are consistent with the infall of the whole dwarf elliptical galaxy population, it is, however, difficult to determine when this happened: the velocity dispersion inside the cluster of their progenitor star-forming, low-luminosity galaxy population should not change very much over a Hubble time as a result of dynamical friction, relaxation, or energy equipartition as shown by Conselice et al. (2001).

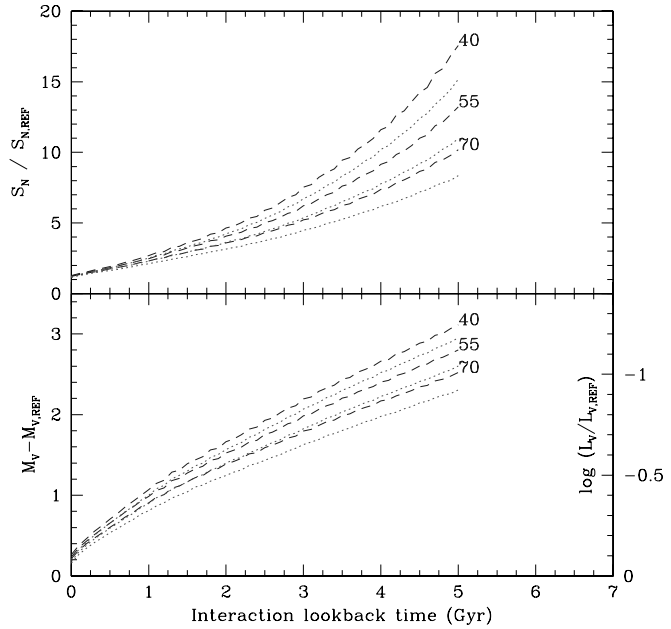

FIG. 18.—Variation of the normalized specific frequency of globular clusters (*top*) and absolute *V*-band magnitude (*bottom*) as a function of the look-back time to the ram pressure stripping event for efficiencies $\epsilon_0 = 0.4$ (*dotted lines*) and 1.2 $M_\odot$ kpc^{-2} yr^{-1} (*dashed lines*) for galaxies characterized by a spin parameter $\lambda = 0.05$ and rotational velocity $V_C = 40$, 55, and 70 km s^{-1} (*top to bottom*). The normalization is made relative to that of a similar unperturbed galaxy. [*See the electronic edition of the Journal for a color version of this figure*.]

6.1.6. *Luminosity Function*

The scenario where all Virgo Cluster early-type dwarfs have been created after the gas removal of low-luminosity late-type galaxies recently infalled into the cluster is, however, too extreme since quiescent dwarf galaxies are present also in the field (Pasquali et al. 2005). The contribution to the faint end of the field luminosity function of dEs, however, is less important than that of blue, star-forming objects (Blanton et al. 2005); it is thus possible that the fraction of dwarf galaxies recently perturbed by the cluster environment is very high. We also remark that the slope of the Virgo Cluster luminosity function ($\alpha \sim -1.4$; Sandage et al. 1985) is comparable to the most recent determinations of the field luminosity function based on SDSS data, $\alpha \sim -1.4$, -1.5 (Blanton et al. 2005). Steeper slopes in other cluster luminosity functions, however, have been determined by Popesso et al. (2006).

6.2. *Infall Rate*

The question now is to see how many Virgo Cluster dwarf ellipticals might have been formed after ram pressure stripping of low-luminosity, star-forming systems. To answer this fundamental question, we should know both the infalling rate of low-luminosity, star-forming galaxies in the cluster and the timescale for a galaxy to totally stop its activity. Our models give us an idea of the different timescales for gas removal and suppression of the star formation

TABLE 3
THE VELOCITY DISTRIBUTION OF DWARF GALAXIES IN VIRGO

	ALL VIRGO					VIRGO A				
CLASS (1)	Mean (km s^{-1}) (2)	σ (km s^{-1}) (3)	Median (km s^{-1}) (4)	Number of Objects (5)	P (%) (6)	Mean (km s^{-1}) (7)	σ (km s^{-1}) (8)	Median (km s^{-1}) (9)	Number of Objects (10)	P (%) (11)
SFD	1362	790	1324	151	4	1166	907	1147	41	82
dE	1201	723	1208	95	72	961	771	943	35	79
dE, N	1168	642	1229	182	3	1120	701	1222	89	12

NOTES.—Col. (1): SFD stands for star-forming dwarfs, low-luminosity ($L_H < 10^{10}\ L_{H\odot}$), high surface brightness [$\mu_e(H) < 22$ mag arcsec^{-2}] late-type galaxies. Cols. (6) and (11): P is the probability that galaxies follow a normal distribution.

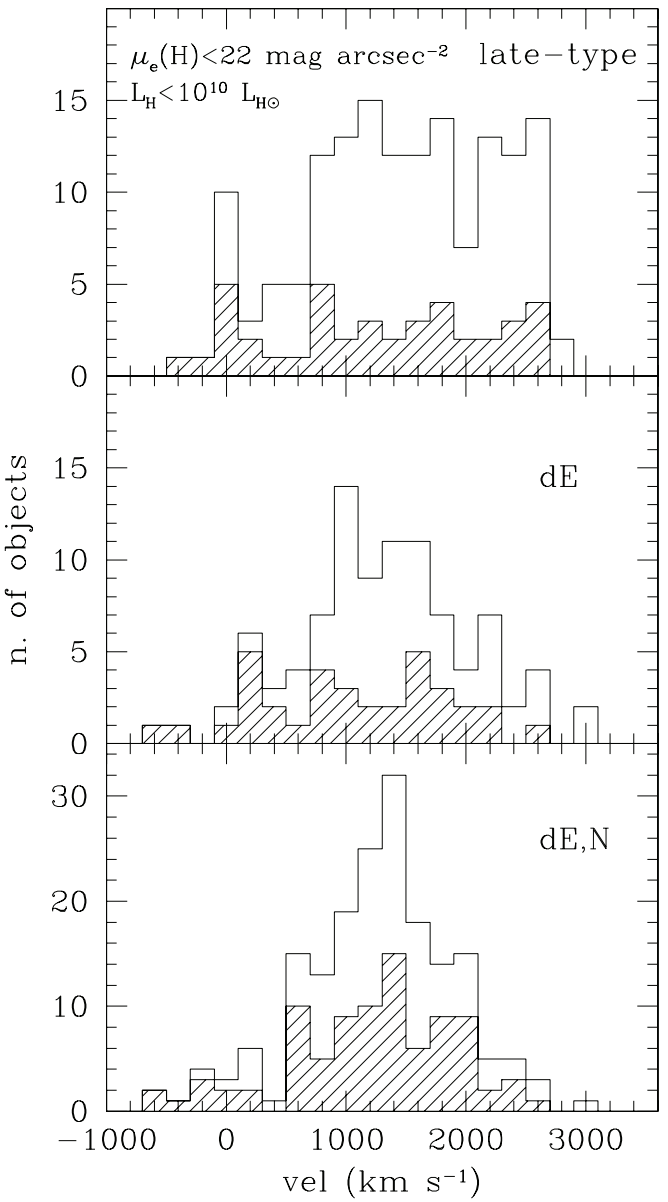

FIG. 19.—Velocity distribution of the low-luminosity ($L_H < 10^{10}\ L_{H\odot}$), high surface brightness [$\mu_e(H) < 22$ mag arcsec^{-2}], star-forming galaxies (*top*) and of nonnucleated (*middle*) and nucleated (*bottom*) dwarf elliptical galaxies in the whole Virgo Cluster region (*open histogram*) and limited to the Virgo A subcluster (*hatched histogram*).

and of the subsequent evolution of the different stellar populations inhabiting these galaxies. Figure 20 shows how, on relatively short timescales, the H I deficiency parameter, on two different indicators tracing the current (Hα emission line; Kennicutt 1998; Boselli et al. 2001) and past (Hβ absorption line[14]; Poggianti & Barbaro 1997; Poggianti et al. 2001a, 2001b; Thomas et al. 2004) star formation activity, and the FUV $-$ H color index are expected to evolve after a ram pressure stripping event for galaxies with $L_H < 10^{9.6}\ L_{H\odot}$. Gas removal is extremely efficient in such low-mass objects, making the H I mass decrease by $\sim$2 orders of magnitude on very short timescales, i.e., $\sim$150 Myr (see Table 5). The lack of gas causes, on similar timescales, a rapid decrease of the Hα EW$_{em}$ (we remind that the Hα emission of a galaxy is due to the gas ionized by O–B stars of ages $<10^7$ yr; Kennicutt 1998). The interaction is so efficient that both indicators are already strongly perturbed even before the galaxy reaches the center of the cluster (look-back time to the interaction = 0 in Fig. 20). The Hβ EW$_{abs}$ and the FUV $-$ H color index, on the other hand, evolve more gradually in time: we can say that on average the equivalent width of the Hβ absorption line drops down to $<$2.8 Å after $\sim$0.5–0.8 Gyr, while FUV $-$ H becomes redder by 5 mag after $\sim$0.8 Gyr independently from the adopted ram pressure stripping model. The transition in between the blue sequence of low-luminosity, star-forming galaxies and the red sequence of quiescent dwarf ellipticals is thus a very rapid event; it is thus not surprising that only a few objects populate the intermediate region.

Table 5 indicates that the fraction of low-luminosity, early-type galaxies in the absolute magnitude range $-13.15 > M_B > -17.5$ (this upper limit roughly corresponds to $L_H < 10^{9.6}\ L_{H\odot}$) with a residual star formation activity (Hα EW$_{em}$ > 2 Å), still rich in H I gas, with a poststarburst activity (Hβ EW$_{abs}$ > 2.8 Å), or with blue colors (FUV $-$ H < 5) is important. These values indicate

[14] This is the absorption line uncontaminated by the Hβ emission, which might be present whenever star formation is still active.

TABLE 4
THE KOLMOGOROV-SMIRNOV TEST FOR RADIAL VELOCITIES

	ALL VIRGO				VIRGO A			
CLASS	E	dE	dE, N	SFD	E	dE	dE, N	SFD
E	100	88	42	4	100	64	36	5
dE	88	100	73	3	64	100	40	40
dE, N	42	73	100	0	36	40	100	41
SFD	4	3	0	100	5	40	41	100

NOTE.—SFD: Star-forming dwarfs are all low-luminosity ($L_H < 10^{10}\ L_{H\odot}$), high surface brightness [$\mu_e(H) < 22$ mag arcsec^{-2}] late-type galaxies.

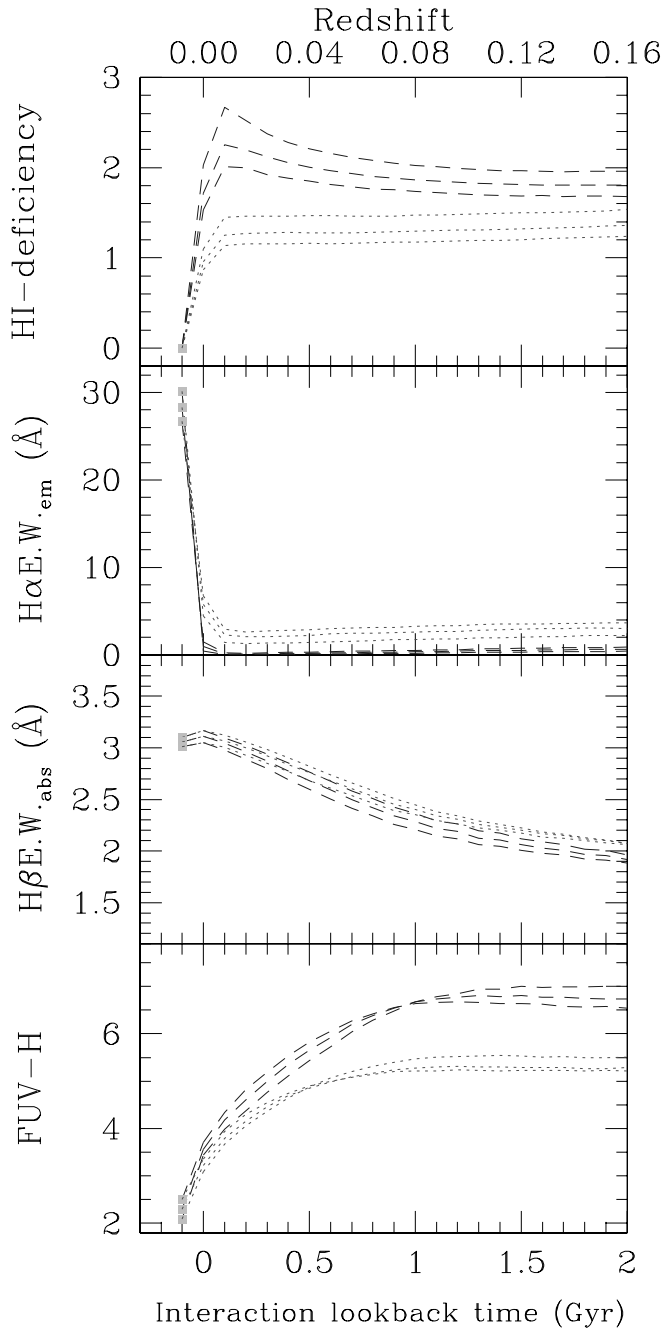

FIG. 20.—Variation of the H I deficiency parameter (*top*), the Hα EW_{em} emission line (*middle top*), the Hβ EW_{abs} absorption line (*middle bottom*), and the FUV $-$ *H* (*bottom*) color index for galaxies with rotational velocities of $V_C = 40$, 55, and 70 km s^{-1} and spin parameter $\lambda = 0.05$ as a function of the look-back time to the interaction. The dotted lines are for a ram pressure stripping model with an efficiency of $\epsilon_0 = 0.4\,M_\odot$ kpc^{-2} yr^{-1}, the dashed lines for a ram pressure stripping model with an efficiency of $\epsilon_0 = 1.2\,M_\odot$ kpc^{-2} yr^{-1}. In both scenarios the efficiency of the perturbation increases with the decrease of the rotational velocity. The look-back time to the interaction (t_{rp}) is equal to zero when the galaxy is currently passing through the cluster center, where ram pressure stripping is at its maximum. Given the extended distribution of the cluster hot gas, the galaxy-ICM interaction in practice starts $\sim$100 Myr before t_{rp}. For this reason, we artificially placed the values for an unperturbed model at $t_{rp} = -100$ Myr (*gray squares*). [*See the electronic edition of the Journal for a color version of this figure*.]

TABLE 5
THE FREQUENCY OF TRANSIENT OBJECTS

Tracer (1)	Condition (2)	Timescale (Myr) (3)	Fraction (*N*/Observed) (4)	Infall Rate (*N*/Gyr) (5)
H I	Non def.	<150	16 (11/68)	475
Hα EW_{em}	>2 Å	<150	10 (31/319)	297
Hβ EW_{abs}	>2.8 Å	<500–800	40 (127/319)[a]	274
FUV $-$ *H*	<5	<800	9 (9/102)[b]	>50

NOTE.—Col. (4): Fraction (total number/observed) of the observed early-type Virgo galaxies with $-13.15 > M_B > -17.5$ satisfying the condition, where the total number of Virgo galaxies satisfying these criteria is 498.

[a] 127 is the total number of galaxies with an Hβ absorption line $\geq$2.8 Å (89) or Hβ in emission (38); if we consider also those with Hα in emission (50), for which the Hβ absorption line is generally underestimated, the total number of objects increases to 148 (46%).

[b] Given the detection limit of *GALEX*, the value relative to the color index FUV $-$ *H* is a lower limit.

that $\sim$10%–16% of the quiescent dwarfs might result from star-forming systems that underwent an interaction with the cluster medium less than 150 Myr ago, while up to $\sim$40% in the last $\sim$500–800 Myr.[15] These values can be used to infer a dwarf galaxy infall rate of $\sim$300 objects Gyr^{-1} (see Table 5), a relatively important rate if we consider the total number of dwarf members of Virgo ($\sim$650; see § 2). This rate, however, is consistent with that determined by Adami et al. (2005) for Coma scaled to the mass of Virgo: $(1–4) \times 10^{12}\,L_\odot$ Gyr^{-1} if a mass-to-light ratio of 10 is adopted.

6.3. *Comparison with Clusters at High z*

These values consistently indicate that the whole Virgo Cluster dwarf quiescent galaxy population might have been formed by the suppression of star formation in low-luminosity, gas-rich systems recently entered into the cluster if an infall rate similar to the present one lasted $\sim$2 Gyr (thus equivalent to $z = 0.16$ in an $H_0 = 70$ km s^{-1} Mpc^{-1}, $\Omega_M = 0.3$, and $\Omega_\lambda = 0.7$ cosmology). This result is consistent with the most recent analysis of the color-magnitude relation of clusters at different redshift that all indicate a significant decrease of the fraction of low-luminosity objects on the red sequence with increasing z (De Lucia et al. 2004, 2007) from $z = 0.24$ (Smail et al. 1998). It has also been shown that the fraction of galaxies in between the red and the blue sequence of the color-magnitude relation (which might be considered as the analogs of our transient population) in high-density environment at $z = 0.7$ from COSMOS increases with the decrease of the galaxy luminosity (Cassata et al. 2007), as predicted by our model. Our results are also consistent with the analysis of Nelan et al. (2005) on 93 nearby clusters based on the age-σ relation, which indicates that the quiescent dwarf galaxy population only recently joined the red sequence.

7. CONCLUSIONS

We can conclude that models and observations are consistent with an evolution of star-forming, low-luminosity, late-type galaxies recently accreted in Virgo into quiescent dwarfs because of the ram pressure gas stripping and the subsequent stopping of

[15] SDSS, Michielsen et al. (2007), and Geha et al. (2003) spectroscopic Hα and Hβ data are limited to the central 3″–4″ of the observed galaxies and are thus not directly comparable to the model predictions, which are relative to the whole galaxy. Integrated spectroscopy, however, is available only for a small fraction of the quiescent dwarfs.

their star formation activity. For consistency with surface brightness measurements, we show that high surface brightness, star-forming dwarf galaxies (low-luminosity spirals and BCD) might be at the origin of the optically selected dwarf ellipticals (both normal and nucleated) analyzed in this work, although we expect that the low surface brightness Magellanic irregulars (Sm and Im), once stripped of their gas reservoir, produce quiescent dwarfs with surface brightnesses below the detection limit of the VCC, as those observed in Virgo by Sabatini et al. (2005). The process of transformation is extremely rapid and efficient, since it works on all dwarfs and lasts on average less than 150 Myr. On longer timescales galaxies get structural and spectrophotometric properties similar to those of dwarf ellipticals. The whole star-forming dwarf galaxy population dominating the faint end of the field luminosity function (Blanton et al. 2005), if accreted, can be totally transformed by the cluster environment into dwarf ellipticals on timescales as short as 2 Gyr and thus be at the origin of the morphology segregation observed also at low luminosities.

This interesting result is of fundamental importance even in a cosmological context because it shows that the majority of dwarf galaxies (if not all of them) are "young" even in clusters, and not old as expected in a hierarchical galaxy formation scenario (see also Nelan et al. 2005). For comparison with De Lucia et al. (2006), we give in Table 6 the look-back time when 50% and 80% of the stars were formed for a model galaxy of $V_C = 55$ km s^{-1} for a (or two) ram pressure stripping event of efficiency $\epsilon_0 = 1.2\ M_\odot$ kpc^{-2} yr^{-1}.

Although the values given in Table 6 are not directly comparable to those given by De Lucia et al. (2006), since they are limited to relatively high mass objects ($2.5 \times 10^9\ M_\odot$, while our model galaxy is of only $2.4 \times 10^8\ M_\odot$), the mean age of the stellar population of low-luminosity, quiescent galaxies is significantly younger than that predicted by hierarchical models of galaxy formation (look-back times $\sim$10 and 8.5 Gyr for 50% and 80% of the stellar population, respectively).

Despite their morphological type, the star formation activity of dwarf systems has been abruptly interrupted by the interaction with the environment in quiescent systems. This conclusion can be extended to the Local Group, where the study of the stellar color-magnitude relation of dwarf spheroidal systems revealed that the star formation activity, although in an episodic manner, lasted for several Gyr (Mateo 1998; Grebel 1999). We can add that the only cluster galaxy population likely to be issued by major merging events, as those predicted by hierarchical models of galaxy formation, is that of massive ellipticals, whose origin is probably very remote ($z \geq 2$–3; Dressler 2004; Treu 2004; Nolan 2004; Franx 2004; Renzini 2006). Indeed this is the only Virgo Cluster galaxy population with a virialized velocity distribution (Conselice et al. 2001). If we consider clusters of galaxies as those regions where merging events were more frequent at early epochs since the big bang just because they were characterized by a high galaxy density, we can conclude that the hierarchical formation scenario was the principal driver of galaxy evolution only in massive objects at very early epochs. All observational evidences are consistent with a secular evolution afterward.

TABLE 6
THE LOOK-BACK TIME TO FORMATION

Model (1)	Time (Myr) (2)	50% (Gyr) (3)	80% (Gyr) (4)
Nonperturbed	...	2.60	0.86
1 crossing	0	2.72	0.98
	500	3.18	1.48
	1000	3.62	1.96
	1500	4.06	2.43
2 crossings	2000	5.98	4.55

NOTES.—Models are for a galaxy $V_C = 55$ km s^{-1} for a (or two) ram pressure stripping event of efficiency $\epsilon_0 = 1.2\ M_\odot$ kpc^{-2} yr^{-1}. Col. (2): Look-back time to the stripping event.

We wish to thank C. Adami, E. Athanassoula, C. Balkowski, V. Buat, G. Comte, P. A. Duc, G. Hensler, J. Lequeux, and H. Wozniak for precious comments and suggestions. We are grateful to the anonymous referee for his constructive suggestions that were extremely useful in the preparation of the final version of the manuscript. *GALEX* (*Galaxy Evolution Explorer*) is a NASA Small Explorer, launched in 2003 April. We gratefully acknowledge NASA's support for construction, operation, and science analysis for the *GALEX* mission, developed in cooperation with the Centre National d'Etudes Spatiales of France and the Korean Ministry of Science and Technology. We wish to thank the *GALEX* SODA team for their help in the data reduction. This research has made use of the GOLDMine database.

APPENDIX A

THE DATA

The data set used in the present analysis is composed of imaging and spectroscopic data covering the whole UV to IR spectral range. The Virgo Cluster region was observed in spring 2004 as part of the All Imaging Survey (AIS) and of the deeper Nearby Galaxy Survey (NGS) carried out by *GALEX* in the two UV bands FUV ($\lambda_{\rm eff} = 1530$ Å, $\Delta\lambda = 400$ Å) and NUV ($\lambda_{\rm eff} = 2310$ Å, $\Delta\lambda = 1000$ Å). This public data set (IR 1.0 release), now available on MAST, has been combined with data extracted from several open time observations obtained at a similar sensitivity as the NGS. Details of the *GALEX* instrument and data characteristics can be found in Martin et al. (2005) and Morrissey et al. (2005).

Whenever available, we extracted fluxes from the NGS and open time images, obtained with an average integration time of $\sim$1500 s. These data are complete to $m_{\rm AB} \sim 21.5$ in the NUV and FUV. Elsewhere UV fluxes have been extracted from the shallower AIS images ($\sim$70 deg^2), obtained with an average integration time of $\sim$100 s, complete to $m_{\rm AB} \sim 20$ in both the FUV and NUV bands.

B and *V* frames are available for most of the analyzed galaxies thanks to our own observations (Gavazzi & Boselli 1996; Gavazzi et al. 2001, 2005b; Boselli et al. 2003). *H* (1.65 μm) and *K* (2.1 μm) frames have been obtained during a near-IR imaging survey of the Virgo Cluster (Boselli et al. 1997b, 2000; Gavazzi et al. 2000b, 2001). SDSS imaging data, taken from the most recent DR5 (release 5; Adelman-McCarthy et al. 2007), have been also used for the determination of the radial NUV $- i$ color gradients.

Fluxes were obtained by integrating all images within elliptical annuli of increasing diameter up to the optical *B*-band 25 mag arcsec^{-2} isophotal radii. Independent measurements of the same galaxies obtained in different exposures give consistent photometric results within

10% in the NUV and 15% in the FUV in the AIS, and about a factor of 2 better for bright (NUV $\leq$ 16) galaxies. We thus estimate that the overall uncertainty in the UV photometry is on average a factor of $\sim$2 better in the NGS or open time images than in the AIS especially for the faintest objects. Optical and near-IR data have on average a photometric accuracy of $\sim$10%. The *H*- and *B*-band structural parameters effective radii R_e (radius containing half of the total light) and surface brightness μ_e (mean surface brightness within R_e) have been measured as described in Gavazzi et al. (2000a). Given the poor resolution of the *GALEX* data (FWHM of the point-spread function $\sim$5″ for a pixel size of 1.5″), these structural parameters are available only for the brightest (and bluest in FUV) dwarf galaxies in Virgo.

Spectral line indices ($H\alpha$ EW_{em}, $H\beta$ EW_{abs}) are available for a large fraction of the analyzed galaxies. Most of the selected objects have been observed as part of a spectroscopic survey of the Virgo Cluster (Gavazzi et al. 2004) still underway. These data have been extracted from long-slit integrated spectroscopy obtained by drifting the slit over the whole galaxy disk, as in Kennicutt (1992), thus providing values representative of the whole object. These are intermediate-resolution ($\lambda/\Delta\lambda \sim 1000$) spectra in the range 3600–7200 Å. Low-resolution spectroscopy of the central region of several galaxies is also available from the SDSS (release 5). To minimize aperture effects, SDSS spectroscopy has been taken only for axisymmetric quiescent galaxies (E, dE, dS0). A few other spectroscopic data for dwarf ellipticals have been taken from Geha et al. (2003) and Michielsen et al. (2007). Line absorption indices ($H\beta$ EW_{abs}) have been measured in the Lick system, although their exact calibration is still underway.

H I data have been taken from the compilation of Gavazzi et al. (2005a), Conselice et al. (2003b), and Giovanelli et al. (2007). The H I deficiency parameter (H I-def) is defined as the logarithmic difference between the average H I mass of a reference sample of isolated galaxies of similar type and linear dimension and the H I mass actually observed in individual objects: H I-def = $\log M_{\rm H\,I,ref} - \log M_{\rm H\,I,obs}$. According to Haynes & Giovanelli (1984), $\log M_{\rm H\,I,ref} = a + b \log(\rm diam)$, where a and b are weak functions of the Hubble type and diam is the linear diameter of the galaxy (see Gavazzi et al. 2005a). Since we make the hypothesis that dwarf ellipticals are gas-stripped, low-luminosity, star-forming objects, their H I deficiency parameter has been determined assuming as reference isolated star-forming dwarf galaxies ($a = 7.00$ and $b = 1.88$, from Gavazzi et al. 2005a). Galaxies with an H I deficiency parameter larger than 0.3 are considered as deficient in H I gas.

Rotational velocities for dwarf elliptical galaxies have been taken from Geha et al. (2003), van Zee et al. (2004b), Pedraz et al. (2002), Thomas et al. (2006), and Simien & Prugniel (1997a, 1997b, 1998, 2002).

UV to near-IR imaging data have been corrected for galactic and internal extinction as described in Boselli et al. (2003). Internal extinction corrections have been applied only to late-type galaxies. Owing to the high galactic latitude of Virgo, galactic extinction corrections are very small ($A_B \leq 0.05$).

Most of the imaging and spectroscopic data used in the present analysis are available in electronic format on the GOLDMine database[16] (Gavazzi et al. 2003).

APPENDIX B

THE MODELS

B1. THE MULTIZONE MODELS FOR THE CHEMICAL AND SPECTROPHOTOMETRIC EVOLUTION OF UNPERTURBED GALAXIES

To trace the evolution of late-type galaxies of different luminosity, we have used the multizone chemospectrophotometric models of Boissier & Prantzos (2000), updated with an empirically determined star formation law (Boissier et al. 2003) relating the star formation rate to the total gas surface densities ($\Sigma_{\rm SFR}$, $\Sigma_{\rm gas}$):

$$\Sigma_{\rm SFR} = \alpha \Sigma_{\rm gas}^{n} V(R)/R, \tag{B1}$$

where $V(R)$ is the rotation velocity at radius R. This is a variant of the traditional "Schmidt law" with two parameters: the index n and an efficiency of the star formation activity α. The values of α and n are taken as equal to 2.63×10^{-3} and 1.48, respectively, as determined from the gaseous and Hα profiles of 16 nearby galaxies (Boissier et al. 2003), where $\Sigma_{\rm SFR}$ is expressed in $M_\odot\,{\rm pc}^{-2}\,{\rm Gyr}^{-1}$, $\Sigma_{\rm gas}$ in $M_\odot\,{\rm pc}^{-2}$, $V(R)$ in km s^{-1}, and R in kpc.

The resulting models are extremely similar to those presented in Boissier & Prantzos (2000) and show the same global trends. We consider the star formation law as fixed, and we keep the same mass accretion (infall) histories as in Boissier & Prantzos (2000), based on the assumption that before the interaction with the cluster, galaxies were "normal" spirals. The free parameters in this grid of models are the spin parameter, λ, and the rotational velocity, V_C. These two parameters are theoretical quantities, although V_C should be similar to the asymptotic value of the rotation curve at large radii. The spin parameter is a dimensionless measure of the specific angular momentum (defined in, e.g., Mo et al. 1998). Its value in spirals ranges typically from $\sim$0.02 for relatively compact galaxies to $\sim$0.09 for low surface brightness galaxies (Boissier & Prantzos 2000). The models of Boissier & Prantzos (2000) contain scaling relationships (the total mass varies as V_C^3, the scale length as λV_C). Star formation histories depend on the infall timescales, which are a function of V_C in these models, so that, roughly speaking, V_C controls the stellar mass accumulated during the history of the galaxy, and λ its radial distribution.

In order to avoid the multiplication of parameters, we decided to fix the spin parameter to an average value of 0.05 and investigate global trends linked to the mass (or the velocity of galaxies) or to the interaction itself. Other values of the spin parameter should mostly create some scatter around these trends. From, e.g., Boissier & Prantzos (2000), it can be seen that trends are mostly driven by mass (see their Fig. 8). Various spin parameters create a modest dispersion with respect to the average one (e.g., about a few tenths of magnitude for the $B - K$ color index, a few tenths of dex for stellar and gaseous masses). The only quantities that are clearly much more affected by

[16] Available at http://goldmine.mib.infn.it.

the spin parameter than the velocity are the surface brightnesses. The central surface brightness in the B band (or r band; see Boissier 2000) can change by a few mag arcsec^{-2} for a given circular velocity when using various realistic spin parameters.

To sample the whole dynamic range covered by dwarf galaxies, we focused our analysis to the velocity range 40–100 km s^{-1}, although we tested several other models for larger velocities (for comparison with bright spirals). We remind that the model, which has a resolution of $\sim$1 kpc, does not include any bulge or nuclear component, corresponding well to pure exponential disks such as these dwarf star-forming galaxies (Gavazzi et al. 2000a). On the other hand, the models were developed and extensively tested for relatively massive galaxies (rotation velocities above 80 km s^{-1}). In this work, we are interested mostly in the 40–100 km s^{-1} range, and low-velocity models were simply extrapolated from the massive ones. By this, we mean that we assumed that the star formation law, initial mass function, and other ingredients used for massive galaxies also apply to the low-mass case. Especially, the models include a dependence of infall timescales on the circular velocity (more massive galaxies form the bulk of their stars earlier than lower mass galaxies). This assumption was found to be in agreement with observations in normal spirals, above $\sim$80 km s^{-1} (Boissier & Prantzos 2000), and is here generalized to lower masses. These considerations call for some caution in the interpretation of our results. Especially, low-mass galaxies are very small and the models do not take into account the likely radial mixing on scales smaller than $\sim$1 kpc, making them extremely uncertain with respect to, e.g., metallicity gradients. Nevertheless, we show in this paper that our extrapolated models reproduce reasonably well the properties of normal late-type, low-velocity galaxies (magnitudes, colors, etc.). In addition, errors due to model uncertainties are likely to be systematic effects: they should affect less differences between two models than absolute values. Thus, we believe that the differences obtained when ram pressure is introduced with respect to the unperturbed case can be trusted.

The models of Boissier & Prantzos (2000) provide total luminosities and colors in all bands, as well as the total gas content. They do not compute the nebular emission, but we estimated the Hα emission by using the number of ionizing photons predicted by Version 5 of Starburst99 (Vázquez & Leitherer 2005) for a single generation of stars distributed on the Kroupa et al. (1993) initial mass function (as used in our models), convolving it with our star formation history, and converting the result into our Hα flux following Appendix A of Gavazzi et al. (2002b).

The models also produce low-resolution theoretical spectra that are used to compute the Lick Hβ index. The model spectral resolution is actually quite poor (20 Å in the visible), but we checked that the evolution of this index in the case of a burst is consistent with the one presented in, e.g., Tantalo & Chiosi (2004).

The evolution of the metallicity is computed in the models taking into account the yields, finite lifetimes of stars, and infall of pristine gas (Boissier & Prantzos 1999). The spectra are computed taking into account this metallicity and the star formation history.

Given the agreement between model predictions and observations for different samples of unperturbed galaxies (Boissier & Prantzos 1999, 2000; Prantzos & Boissier 2000; Boissier et al. 2001), we consider them as the reference models for the unperturbed case. As for NGC 4569 (Boselli et al. 2006), we study two different interaction scenarios, starvation and ram pressure stripping.

B2. THE STARVATION SCENARIO

In the starvation scenario (Larson et al. 1980; Balogh et al. 2000; Treu et al. 2003), the cluster acts on large scales by removing any extended gaseous halo surrounding the galaxy, preventing further infall of such gas onto the disk. The galaxy then becomes anemic simply because it exhausts the gas reservoir through ongoing star formation.

Infall is a necessary assumption in models of the chemical evolution of the Milky Way to account for the G dwarf metallicity distribution (Tinsley 1980) and is supported by some chemodynamical models (Samland et al. 1997). As the disk galaxy models were obtained through a generalization of the Milky Way model, infall is present in all our models. It is a schematic way to describe the growth of any galaxy from a protogalactic clump in the distant past to a present-day galaxy. Infall timescales in the models were chosen to reproduce the properties of present-day normal galaxies (Boissier & Prantzos 2000; Boissier et al. 2001). This includes a dependency on the rotational velocity such that infall in low-mass galaxies is shifted toward later time: this mimics the fact that massive galaxies are formed early on and that low-mass galaxies are still forming at the current time, a well-known fact (Gavazzi et al. 1996, 2002a; Boselli et al. 2001) nowadays called "downsizing." Because of this effect, low-mass galaxies, in the absence of interaction, are accreting large amounts of gas and are still actively forming stars. In the event of starvation, the galaxy stops accreting gas and continues forming stars from the reservoir already present in the disk. This proceeds at a lower rate than in the unperturbed case, with a declining activity in time as the consumed gas is not replaced with fresh gas. Stopping infall (in order to mimic starvation) at a given time is straightforward to include in the model. We call t_s the elapsed time since the infall termination (look-back time).

B3. THE RAM PRESSURE STRIPPING SCENARIO

In addition to the starvation scenario, we can study the effect of ram pressure gas stripping. As in Boselli et al. (2006), we adopt the plausible scenario of Vollmer et al. (2001) explicitly tailored to Virgo; i.e., the galaxies being modeled have crossed the dense IGM only once (in its simplest version), on elliptical orbits. The ram pressure exerted by the IGM on the galaxy ISM varies in time following a Gaussian profile, whose peak at $t = t_{\rm rp}$ is when the galaxy is crossing the dense cluster core at high velocity (t and $t_{\rm rp}$ are look-back times, where the present epoch corresponds to $t = 0$). The Gaussian has a width $\Delta t = 9 \times 10^7$ yr (see Fig. 3 of Vollmer et al. 2001). We make the hypothesis that the gas at each radius is removed at a rate that is directly proportional to the galaxy gas column density $\Sigma_{\rm gas}$ and inversely proportional to the potential of the galaxy, measured by the total (baryonic) local density $\Sigma_{\rm potential}$ (provided by the model). The gas-loss rate adopted is then equal to $\epsilon(\Sigma_{\rm gas}/\Sigma_{\rm potential})$, with the efficiency ϵ following a Gaussian having a maximum ϵ_0 at the time $t_{\rm rp}$, chosen to mimic the variation of the ram pressure suggested by Vollmer et al. (2001). This very simple but physically motivated prescription should allow us to model the gas removal from galaxies using only two free parameters ($t_{\rm rp}$ and ϵ_0) to age-date and measure the magnitude of this effect. To further constrain the models, we assume two different values of ϵ_0: the first is $\epsilon_0 = 1.2\ M_\odot$ kpc^{-2} yr^{-1}, the value best reproducing the radial profiles of NGC 4569 (Boselli et al. 2006); the second one is one-third of it, $\epsilon_0 = 0.4\ M_\odot$ kpc^{-2} yr^{-1}. This second value is suggested by the following considerations: besides the potential of the galaxy, which is an intrinsic property of each

object, the efficiency of ram pressure (P) stripping depends on the density of the cluster IGM ($\rho_{\rm IGM}$), on the crossing velocity of the galaxy within the cluster ($V_{\rm gal}$), and on its orientation with respect to its motion (Boselli & Gavazzi 2006): $P = \rho_{\rm IGM} V_{\rm gal}^2$. Statistically speaking, the line-of-sight velocity dispersion of star-forming galaxies in the cluster is 1150 km s^{-1} and drops to 766 km s^{-1} if limited to low-luminosity star-forming objects in the Virgo A subgroup from where the X-ray emission comes. These values can be compared to the line-of-sight velocity of NGC 4569 with respect to the cluster center, which is 1374 km s^{-1}. To test other realistic models, we thus decided to use an ϵ_0 lower by a factor of $\sim(1374/766)^2 = 3.2$ than in NGC 4569. The value $\epsilon_0 = 0.4\ M_\odot$ kpc^{-2} yr^{-1} can thus be considered as an average value of relatively weak interactions, while $\epsilon_0 = 1.2\ M_\odot$ kpc^{-2} yr^{-1} is a realistic value representative of more extreme interactions. As we discuss in the main body of the paper, $\epsilon_0 = 0.4\ M_\odot$ kpc^{-2} yr^{-1} leads to H I deficiency parameters of $\sim$0.8 for massive galaxies, consistent with the average H I deficiency observed within one virial radius in Virgo, while $\epsilon_0 = 1.2\ M_\odot$ kpc^{-2} yr^{-1} to H I deficiencies of $\sim$1.5, close to the highest values found in Virgo (Gavazzi et al. 2005a; Boselli & Gavazzi 2006). In massive galaxies H I deficiencies as high as $\sim$2 have been observed (Gavazzi et al. 2005a) and are probably the result of stripping events more efficient than those simulated. These extreme H I deficiencies can also be the result of subsequent crossings of the cluster center, which should happen on average every $\sim$1.7 Gyr (Boselli & Gavazzi 2006). Multiple crossing can be reproduced by our models just considering that the average crossing time of star-forming galaxies in the Virgo Cluster is 1.7 Gyr (Boselli & Gavazzi 2006).

We make the further assumption that no extra star formation is induced during the interaction. This assumption is reasonable since ram pressure stripping models of Fujita (1998) and Fujita & Nagashima (1999) indicate that on short timescales ($\sim 10^8$ yr) the star formation activity of galaxies can increase by up to a factor of 70% at most in high-density, rich clusters such as Coma, but it decreases to values lower than before the interaction whenever the density of the IGM is relatively low as in the core of Virgo. Indeed, we do not have any evidence of a statistically significant increase of the star formation activity in galaxies that recently underwent a ram pressure stripping event (Iglesias-Paramo et al. 2004). Given the rapidity of the gas stripping process (150 Myr; see § 5.2) in these dwarf systems, a possible mild increase of their star formation activity does not have enough time to produce significant modification in their spectrophotometric and structural properties.

REFERENCES

Adami, C., Biviano, A., Durret, F., & Mazure, A. 2005, A&A, 443, 17
Adelman-McCarthy, J., et al. 2007, ApJS, 172, 634
Auld, R., et al. 2006, MNRAS, 371, 1617
Balogh, M. L., Navarro, J. F., & Morris, S. L. 2000, ApJ, 540, 113
Bender, R., Burstein, D., & Faber, S. 1992, ApJ, 399, 462
Binggeli, B., & Popescu, C. 1995, A&A, 298, 63
Binggeli, B., Popescu, C., & Tammann, G. 1993, A&AS, 98, 275
Binggeli, B., Sandage, A., & Tammann, G. 1985, AJ, 90, 1681
———. 1988, ARA&A, 26, 509
Binggeli, B., Tarenghi, M., & Sandage, A. 1990, A&A, 228, 42
Blanton, M. R., Lupton, R., Schleghel, D., Strauss, M., Brinkmann, J., Fukugita, M., & Loveday, J. 2005, ApJ, 631, 208
Boissier, S. 2000, Ph.D. thesis, Institut d'Astrophysique de Paris
Boissier, S., Boselli, A., Prantzos, N., & Gavazzi, G. 2001, MNRAS, 321, 733
Boissier, S., & Prantzos, N. 1999, MNRAS, 307, 857
———. 2000, MNRAS, 312, 398
Boissier, S., Prantzos, N., Boselli, A., & Gavazzi, G. 2003, MNRAS, 346, 1215
Boselli, A. 1994, A&A, 292, 1
Boselli, A., Boissier, S., Cortese, L., Gil de Paz, A., Seibert, M., Madore, B. F., Buat, V., & Martin, D. C. 2006, ApJ, 651, 811
Boselli, A., & Gavazzi, G. 2006, PASP, 118, 517
Boselli, A., Gavazzi, G., Combes, F., Lequeux, J., & Casoli, F. 1994, A&A, 285, 69
Boselli, A., Gavazzi, G., Donas, J., & Scodeggio, M. 2001, AJ, 121, 753
Boselli, A., Gavazzi, G., Franzetti, P., Pierini, D., & Scodeggio, M. 2000, A&AS, 142, 73
Boselli, A., Gavazzi, G., Lequeux, J., Buat, V., Casoli, F., Dickey, J., & Donas, J. 1997a, A&A, 327, 522
Boselli, A., Gavazzi, G., & Sanvito, G. 2003, A&A, 402, 37
Boselli, A., Lequeux, J., & Gavazzi, G. 2002, A&A, 384, 33
Boselli, A., Tuffs, R., Gavazzi, G., Hippelein, H., & Pierini, D. 1997b, A&AS, 121, 507
Boselli, A., et al. 2005a, ApJ, 623, L13
———. 2005b, ApJ, 629, L29
Bothun, G., Mould, J., Caldwell, N., & MacGillivray, H. 1986, AJ, 92, 1007
Bower, R. G., Lucey, J. R., & Ellis, R. S. 1992, MNRAS, 254, 601
Buat, V., & Xu, K. 1996, A&A, 306, 61
Bullock, J., Kravtsov, A., & Weinberg, D. 2000, ApJ, 539, 517
Cassata, P., et al. 2007, ApJS, 172, 270
Catinella, B., Giovanelli, R., & Haynes, M. 2006, ApJ, 640, 751
Cole, S., Aragon-Salamanca, A., Frenk, C., Navarro, J., & Zepf, S. 1994, MNRAS, 271, 781
Conselice, C. 2002, ApJ, 573, L5
Conselice, C., Gallagher, J., & Wyse, R. 2001, ApJ, 559, 791
———. 2003a, AJ, 125, 66
Conselice, C., O'Neil, K., Gallagher, J., & Wyse, R. 2003b, ApJ, 591, 167
Côté, P., et al. 2006, ApJS, 165, 57
Davies, J., & Phillipps, S. 1988, MNRAS, 233, 553
Dekel, A., & Silk, J. 1986, ApJ, 303, 39
De Lucia, G., Springel, V., White, S., Croton, D., & Kauffmann, G. 2006, MNRAS, 366, 499
De Lucia, G., et al. 2004, ApJ, 610, L77
———. 2007, MNRAS, 374, 809
Dressler, A. 1980, ApJ, 236, 351
———. 2004, in Clusters of Galaxies: Probes of Cosmological Structure and Galaxy Evolution, ed. J. S. Mulchaey, A. Dressler, & A. Oemler (Cambridge: Cambridge Univ. Press), 206
Duc, P.-A., Cayatte, V., Balkowski, C., Thuan, T. X., Papaderos, P., & van Driel, W. 2001, A&A, 369, 763
Elmegreen, D., Elmegreen, B., Frogel, J., Eskridge, P., Pogge, R., Gallager, A., & Iams, J. 2002, AJ, 124, 777
Ferguson, H., & Binggeli, B. 1994, A&A Rev., 6, 67
Ferrara, A., & Tolstoy, E. 2000, MNRAS, 313, 291
Franx, M. 2004, in Clusters of Galaxies: Probes of Cosmological Structure and Galaxy Evolution, ed. J. S. Mulchaey, A. Dressler, & A. Oemler (Cambridge: Cambridge Univ. Press), 196
Fuchs, B., & von Linden, S. 1998, MNRAS, 294, 513
Fujita, Y. 1998, ApJ, 509, 587
Fujita, Y., & Nagashima, M. 1999, ApJ, 516, 619
Gavazzi, G., Bonfanti, C., Sanvito, G., Boselli, A., & Scodeggio, M. 2002a, ApJ, 576, 135
Gavazzi, G., & Boselli, A. 1996, Astrophys. Lett. Commun., 35, 1
———. 1999, A&A, 343, 93
Gavazzi, G., Boselli, A., Cortese, L., Arosio, I., Gallazzi, A., Pedotti, P., & Carrasco, L. 2006a, A&A, 446, 839
Gavazzi, G., Boselli, A., Donati, A., Franzetti, P., & Scodeggio, M. 2003, A&A, 400, 451
Gavazzi, G., Boselli, A., & Kennicutt, R. 1991, AJ, 101, 1207
Gavazzi, G., Boselli, A., Pedotti, P., Gallazzi, A., & Carrasco, L. 2002b, A&A, 396, 449
Gavazzi, G., Boselli, A., Scodeggio, M., Pierini, D., & Belsole, E. 1999, MNRAS, 304, 595
Gavazzi, G., Boselli, A., van Driel, W., & O'Neil, K. 2005a, A&A, 429, 439
Gavazzi, G., Catinella, B., Carrasco, L., Boselli, A., & Contursi, A. 1998, AJ, 115, 1745
Gavazzi, G., Donati, A., Cuccati, O., Sabatini, S., Boselli, A., Davies, J., & Zibetti, S. 2005b, A&A, 430, 411
Gavazzi, G., Franzetti, P., Scodeggio, M., Boselli, A., & Pierini, D. 2000a, A&A, 361, 863
Gavazzi, G., Franzetti, P., Scodeggio, M., Boselli, A., Pierini, D., Baffa, C., Lisi, F., & Hunt, L. 2000b, A&AS, 142, 65
Gavazzi, G., O'Neil, K., Boselli, A., & van Driel, W. 2006b, A&A, 449, 929
Gavazzi, G., Pierini, D., & Boselli, A. 1996, A&A, 312, 397
Gavazzi, G., Zaccardo, A., Sanvito, G., Boselli, A., & Bonfanti, C. 2004, A&A, 417, 499
Gavazzi, G., Zibetti, S., Boselli, A., Franzetti, P., Scodeggio, M., & Martocchi, S. 2001, A&A, 372, 29

Geha, M., Guhathakurta, P., & van der Marel, R. P. 2003, AJ, 126, 1794
Gil de Paz, A., et al. 2007, ApJS, 173, 185
Giovanelli, R., et al. 2005, AJ, 130, 2598
———. 2007, AJ, 133, 2569
Graham, A., & Guzman, R. 2003, AJ, 125, 2936
Graham, A., Jerjen, H., & Guzman, R. 2003, AJ, 126, 1787
Grebel, E. 1999, in IAU Symp. 192, The Stellar Content of Local Group Galaxies, ed. P. Whitelock & R. Cannon (San Francisco: ASP), 17
Grebel, E., Gallagher, J., & Harbeck, D. 2003, AJ, 125, 1926
Gunn, J. E., & Gott, J. R. I. 1972, ApJ, 176, 1
Haynes, M., & Giovanelli, R. 1984, AJ, 89, 758
Iglesias-Paramo, J., Boselli, A., Gavazzi, G., & Zaccardo, A. 2004, A&A, 421, 887
Kauffmann, G., White, S., & Guiderdoni, B. 1993, MNRAS, 264, 201
Kennicutt, R. C., Jr. 1992, ApJ, 388, 310
———. 1998, ARA&A, 36, 189
Klypin, A., Kravtsov, A., Valenzuela, O., & Prada, F. 1999, ApJ, 522, 82
Kroupa, P., Tout, C. A., & Gilmore, G. 1993, MNRAS, 262, 545
Larson, R., Tinsley, B., & Caldwell, N. 1980, ApJ, 237, 692
Lin, D., & Faber, S. 1983, ApJ, 266, L21
Lisker, T., Glatt, K., Westera, P., & Grebel, E. 2006a, AJ, 132, 2432
Lisker, T., Grebel, E., & Binggeli, B. 2006b, AJ, 132, 497
Lisker, T., Grebel, E., Binggeli, B., & Glatt, K. 2007, ApJ, 660, 1186
Lotz, J., Miller, B., & Ferguson, H. 2004, ApJ, 613, 262
Mac Low, M., & Ferrara, A. 1999, ApJ, 513, 142
Marcolini, A., Brighenti, F., & D'Ercole, A. 2003, MNRAS, 345, 1329
Martin, C., et al. 2005, ApJ, 619, L1
Mastropietro, C., Moore, B., Mayer, L., Debattista, V., Piffaretti, R., & Stadel, J. 2005, MNRAS, 364, 607
Mateo, M. 1998, ARA&A, 36, 435
Mayer, L., Governato, F., Colpi, M., Moore, B., Quinn, T., Wadsley, J., Stadel, J., & Lake, G. 2001a, ApJ, 547, L123
———. 2001b, ApJ, 559, 754
Michielsen, D., et al. 2007, MNRAS, in press (arXiv:0712.2017)
Miller, B., Lotz, J., Ferguson, H., Stiavelli, M., & Whitmore, B. 1998, ApJ, 508, L133
Mo, H. J., Mao, S., & White, S. D. M. 1998, MNRAS, 295, 319
Moore, B., Lake, G., & Katz, N. 1998, ApJ, 495, 139
Mori, M., & Burkert, A. 2000, ApJ, 538, 559
Morrissey, P., et al. 2005, ApJ, 619, L7
Murakami, I., & Babul, A. 1999, MNRAS, 309, 161
Nagashima, M., Yahgi, H., Enoki, M., Yoshii, Y., & Gouda, N. 2005, ApJ, 634, 26
Nelan, J., Smith, R., Hudson, M., Wegner, G., Lucey, J., Moore, S., Quinney, S., & Suntzeff, N. 2005, ApJ, 632, 137
Nolan, L. A. 2004, in Clusters of Galaxies: Probes of Cosmological Structure and Galaxy Evolution, ed. J. S. Mulchaey, A. Dressler, & A. Oemler (Cambridge: Cambridge Univ. Press), 38
Pasquali, A., Larsen, S., Ferreras, I., Gnedin, O., Malhotra, S., Rhoads, J., Pirzkal, N., & Walsh, J. 2005, AJ, 129, 148
Pedraz, S., Gorgas, J., Cardiel, N., Sánchez-Blásquez, P., & Guzmán, R. 2002, MNRAS, 332, L59
Poggianti, B. M., & Barbaro, G. 1997, A&A, 325, 1025
Poggianti, B. M., et al. 2001a, ApJ, 562, 689
———. 2001b, ApJ, 563, 118
Popesso, P., Biviano, A., Böringer, H., & Romaniello, M. 2006, A&A, 445, 29
Prantzos, N. 2000, NewA Rev., 44, 303
Prantzos, N., & Boissier, S. 2000, MNRAS, 313, 338
Renzini, A. 2006, ARA&A, 44, 141
Sabatini, S., Davies, J., van Driel, W., Baes, M., Roberts, S., Smith, R., Linder, S., & O'Neil, K. 2005, MNRAS, 357, 819
Samland, M., Hensler, G., & Theis, C. 1997, ApJ, 476, 544
Sandage, A., Binggeli, B., & Tammann, G. 1985, AJ, 90, 1759
Scodeggio, M., Gavazzi, G., Franzetti, P., Boselli, A., Zibetti, S., & Pierini, D. 2002, A&A, 384, 812
Sellwood, J., & Carlberg, R. 1984, ApJ, 282, 61
Seth, A., Dalcanton, J., & de Jong, R. 2005, AJ, 130, 1574
Silich, S., & Tenorio-Tagle, G. 1998, MNRAS, 299, 249
———. 2001, ApJ, 552, 91
Simien, F., & Prugniel, P. 1997a, A&AS, 122, 521
———. 1997b, A&AS, 126, 15
———. 1998, A&AS, 131, 287
———. 2002, A&A, 384, 371
Smail, I., Edge, A., Ellis, R., & Blandford, R. 1998, MNRAS, 293, 124
Somerville, R., & Primack, J. 1999, MNRAS, 310, 1087
Strader, J., Brodie, J., Spitler, L., & Beasley, M. 2006, AJ, 132, 2333
Tantalo, R., & Chiosi, C. 2004, MNRAS, 353, 917
Thomas, D., Brimioulle, F., Bender, R., Hopp, U., Greggio, L., Maraston, C., & Saglia, R. 2006, A&A, 445, L19
Thomas, D., Maraston, C., & Korn, A. 2004, MNRAS, 351, L19
Tinsley, B. M. 1980, Fundam. Cosm. Phys., 5, 287
Treu, T. 2004, in Clusters of Galaxies: Probes of Cosmological Structure and Galaxy Evolution, ed. J. S. Mulchaey, A. Dressler, & A. Oemler (Cambridge: Cambridge Univ. Press), 177
Treu, T., Ellis, R. S., Kneib, J.-P., Dressler, A., Smail, I., Czoske, O., Oemler, A., & Natarajan, P. 2003, ApJ, 591, 53
Tully, B., Mould, J., & Aaronson, M. 1982, ApJ, 257, 527
Vader, J. 1986, ApJ, 305, 669
van Zee, L., Barton, E., & Skillman, E. 2004a, AJ, 128, 2797
van Zee, L., Skillman, E., & Haynes, M. 2004b, AJ, 128, 121
Vázquez, G. A., & Leitherer, C. 2005, ApJ, 621, 695
Vilchez, J. M. 1995, AJ, 110, 1090
Visvanathan, N., & Sandage, A. 1977, ApJ, 216, 214
Vollmer, B., Cayatte, V., Balkowski, C., & Duschl, W. 2001, ApJ, 561, 708
White, S., & Frenk, C. 1991, ApJ, 379, 52
White, S., & Rees, M. 1978, MNRAS, 183, 341
Yoshii, Y., & Arimoto, N. 1987, A&A, 188, 13